colloids and interfaces

MDPI

Article

A Selective, Efficient, Facile, and Reusable Natural Clay/Metal Organic Framework as a Promising Adsorbent for the Removal of Drug Residue and Heavy Metal Ions

Rania Abdelazeem [1], Heba A. Younes [1], Zienab E. Eldin [2], Ahmed A. Allam [3,4], Hassan Ahmed Rudayni [4], Sarah I. Othman [5], Ahmed A. Farghali [2], Hamada M. Mahmoud [3] and Rehab Mahmoud [6,*]

1 Environmental Science and Industrial Development Department, Faculty of Postgraduate Studies for Advanced Sciences, Beni-Suef University, Beni-Suef 62521, Egypt
2 Materials Science and Nanotechnology Department, Faculty of Postgraduate Studies for Advanced Science (PSAS), Beni-Suef University, Beni-Suef 62511, Egypt
3 Zoology Department, Faculty of Science, Beni-Suef University, Beni-Suef 62511, Egypt
4 Department of Biology, College of Science, Imam Mohammad bin Saud Islamic University, Riyadh 11623, Saudi Arabia
5 Department of Biology, College of Science, Princess Nourah bint Abdulrahman University, Riyadh 11671, Saudi Arabia
6 Department of Chemistry, Faculty of Science, Beni-Suef University, Beni-Suef 62511, Egypt
* Correspondence: rehabkhaled@science.bsu.edu.eg

Abstract: It is imperative to eliminate heavy metals and pharmaceutical residual pollutants from wastewater to reduce their detrimental effects on the environment. In this work, natural zeolite and a 2-amino terephthalic acid-based multi-metallic organic framework were used to create a new composite that can be utilized as an adsorbent for cadmium and safinamide. The adsorption study was examined in a variety of settings (pH, adsorbent dosage, pollutant concentration, and time). Moreover, Zeta potential, BET, SEM, FTIR, XRD, and SEM measurements were used to characterize the adsorbents. The adsorption process was confirmed using FTIR, XRD, and SEM analysis. Various nonlinear adsorption isotherm models were applied to adsorption results. The results showed a significantly better adsorption ability for safinamide and cadmium using zeolite/MOF compared to zeolite. Adsorption kinetics were represented by five models: pseudo first-order, pseudo second-order, intraparticle diffusion, mixed first- and second-order, and the Avrami model. Regarding both adsorbent substances, safinamide adsorption was best represented by the intraparticle diffusion model. In contrast, the pseudo second-order and intraparticle diffusion models for zeolite and zeolite/MOF, respectively, better fit the experimental results in the case of cadmium adsorption. The thermodynamic parameters ΔH°, ΔS°, and ΔG° were investigated through temperature tests carried out at 25, 35, 45, and 55 °C. Exothermic and spontaneous adsorption processes were demonstrated by the computed values. The study of adsorbent regeneration involved the use of several chemical solvents. The DMSO solvent was shown to have the highest adsorbent regeneration method efficiency at 63%. Safinamide elimination was lessened by organic interfering species like cefixime and humic acid compared to inorganic species like chloride, sulphate, and nitrate, most likely as a result of intense competition for the few available active sites. Using zeolite/MOF nanocomposite, the percentage of safinamide removed from spiked real water samples (tap water, Nile River water, and groundwater samples) was 48.80%, 64.30%, and 44.44%, respectively. Based on cytotoxicity results, the highest percentages of cell viability for zeolite and zeolite/MOF at 24 h were 83% and 81%, respectively, in comparison to untreated controls. According to these results, zeolite and zeolite/MOF composites can be used as effective adsorbents for these pollutants in wastewater.

Keywords: safinamide; wastewater; zeolite; MOF; adsorption; heavy metals

Citation: Abdelazeem, R.; Younes, H.A.; Eldin, Z.E.; Allam, A.A.; Rudayni, H.A.; Othman, S.I.; Farghali, A.A.; Mahmoud, H.M.; Mahmoud, R. A Selective, Efficient, Facile, and Reusable Natural Clay/Metal Organic Framework as a Promising Adsorbent for the Removal of Drug Residue and Heavy Metal Ions. *Colloids Interfaces* **2024**, *8*, 50. https://doi.org/10.3390/colloids8050050

Academic Editor: Reinhard Miller

Received: 10 July 2024
Revised: 16 August 2024
Accepted: 27 August 2024
Published: 5 September 2024

1. Introduction

Numerous environmental problems, particularly water pollution, have emerged with population growth and industrialization [1]. The primary water pollutants affecting the ecosystem are organic compounds and heavy metals [2,3]. Pharmaceuticals are organic micropollutants with high toxicity and low biodegradability, which may adversely affect aquatic life. Such organic compounds can cause hyperactivity, delayed hatching, and increased body size in zebrafish embryos [4,5]. Many studies have shown that annual wastewater releases roughly 300 tonnes of various micropollutants, including pesticides and industrial chemicals, into the environment [6,7]. Heavy metal pollutants, such as cadmium, cobalt, copper, chromium, nickel, and lead, are released into surface water bodies through industrial effluents, posing a threat to living organisms [8]. These toxic substances can lead to various health issues, including cancer, organ shrinkage, immune and neurological dysfunction, and even fatal illnesses [9,10]. Therefore, using simple, cost-effective techniques, pharmaceuticals and heavy metals should be removed efficiently from water streams [11]. Different methods, such as adsorption, biodegradation, ozonation [8], photocatalysis, membrane filtering, coagulation, and flocculation, have been employed to treat pharmaceutical wastewater and heavy metals [12–16]. Each method has advantages and disadvantages, such as generating hazardous by-products in the catalysis method and the costly nature of operation and maintenance [17]. Adsorption is a promising technique for removing various pollutants from wastewater since it is an effective and low-cost method. In addition, adsorption is a versatile technique since adsorbents' properties may be changed by modifying their surfaces' hydrophobicity, reactivity, surface energy, surface loading, roughness, and surface area [9]. Many effective adsorbents are applied for pharmaceuticals and heavy metals such as activated carbon, metal-organic frameworks, and biomass. For the majority of the last few decades, activated carbon has been utilized as an adsorbent to recover industrial and municipal wastewater. However, the high price of activated carbon has motivated researchers to look for appropriate, less expensive adsorbents, particularly in developing nations [18]. These adsorbents' principal drawback is their lacklustre selectivity. Furthermore, the random pore that may impede the target metal ion's efficient transport contributes to the comparatively low adsorption kinetic. Additionally, because of their weak coordination chemistry with the metal ion, treatment is needed for the metal ion, such as acidification and impregnation to a particular group that increases the adsorption capacity and selectivity [11]. Because of this, current research has concentrated on creating affordable substitutes utilizing a variety of natural resources and industrial wastes [19].

Natural substances include silica and zeolite [20–24]. Natural zeolites are hydrated aluminosilicate materials with varying pore sizes and are suitable for ion exchange, adsorption, and dehydration [25]. Due to their wide availability and diverse properties, natural zeolites have been extensively studied and exploited [26,27]. MOFs' huge specific surface area, high porosity, variety of functionalities, and good thermal stability have piqued the curiosity of researchers studying adsorption applications. Pollutant diffusion on the skeleton and the accessibility of adsorption sites are facilitated by a large specific surface area and high porosity. Simultaneously, MOF metal composites could be created by carefully choosing organic connectors and connecting them to metal nodes, which would improve the adsorption capacity and recovery in addition to adjusting the size and shape of pores. Due to these unusual characteristics, the last few years have seen a surge in research interest in the field of MOF-based materials, and this class of materials has also been investigated as a potential novel platform for the adsorption and removal of contaminants in water media [19]. Zeolite (as a cheap alternative) and MOF (as an advanced, efficient adsorbent) were combined in a nanocomposite that was investigated as an adsorbent to remove cadmium as a representative example of a heavy metal (Table 1) and safinamide as an example of a pharmaceutical. In this work, a multi-metallic MOF was prepared and supported on natural zeolite to form a composite. They were characterized, and their removal efficiency for both safinamide and cadmium was investigated.

Table 1. Studies reporting the adsorption of Cd^{2+} on zeolite- and MOF-based adsorbents compared to the current study.

Adsorbent	pH	Equilibrium Time (min)	Adsorbent Dose	Removal Percent (%)	q_{max} (mg/g)	Reference
TMU-5 metal organic framework	7	-	15 mg/L	-	1929	[28]
MoS_4-Cu-BTC	-	30	-	-	833.3	[29]
CaFu-MOF	7	350	-	-	781.2	[29]
Fe_3O_4@UiO-66–NH_2	6	300	-	-	714.3	[30]
MIL-53(Fe)-1	-	50	-	-	714.28	[31]
Amino-decorated magnetic metal-organic framework	7	20	0.05 g	-	693	[31]
silica-coated metal organic framework	6	-	15 mg/L	-	634	[28]
Co/Ni/Cu-NH_2BDC MOF/natural Zeolite ore	9	25			550.69	This work
PAN/chitosan/UiO-66-NH_2 nanofibers	-	90	-	-	415.6	[29]
UiO-66@mSi-SO_3H	7		100 mg/L	-	410	[28]
Fe_3O_4@ZIF-8	6	300	-	-	370	[30]
Corn Silk/Corn Silk/Zeolite-Y	5	7	0.009 g	-	315.27	[32]
zeolitic imidazolate framework-8	7	240	20 mg	80	312.5	[33]
Bimetallic Ag–Fe MOF	7	120	-	-	265	[34]
zeolitic imidazolate framework-8	7	15	20 mg	40	263.16	[33]
Cu-MOF	-	60	0.5 g	98.62	219.05	[35]
magnetic zeolite	5	240	-	-	204.2	[36]
UiO-66 MOF modified with Melamine	5	50	1 g/L	84	146.6	[37]
TMU-16-NH_2 MOF	6	30	0.05 g	98.91	126.6	[38]
zeolite NaX	5	120	2 g/L	>90%	100.11	[39]
Zeolite from oil shale ash	-	-	-	-	95.6	[40]
SO_3H Functionalized $Cu_3(BTC)_2$ MOF	6	10	1 mg/mL	99	88.7	[41]
natural clinoptilolite zeolite decorated by Fe_3O_4 nanoparticles	6	60	1 g/L	68.9	19.9	[42]
Na- and Fe-modified zeolitic tuffs	6	420	-	-	18	[43]
Iranian natural zeolite	3	1440	1 g	>90%	4	[44]

2. Materials and Methods

2.1. Chemicals

Natural Egyptian zeolite ore was collected from the northwestern region of Beni-Suef Governorate (N 29°25′12″, E 31°9′36″). Copper nitrate ($Cu(NO_3)_2{\cdot}3H_2O$), cobalt nitrate ($Co(NO_3)_2{\cdot}6H_2O$), and nickel nitrate ($Ni(NO_3)_2{\cdot}6H_2O$) were acquired from Loba Chemie, Piochem, and Alpha Chemika, respectively. 2-amino terephthalic acid and N,N dimethyl formamide were purchased from Sigma Aldrich and Carlo Erba. A 1000 ppm standard cadmium solution was obtained from Scharlab.

2.2. Synthesis of Co/Ni/Cu-NH_2BDC MOF Metal-Organic Frameworks

Co/Ni/Cu-NH_2BDC MOF was prepared using a simple solvothermal technique where 2-amino terephthalic acid (3 mmol) was dissolved in 120 mL of N,N-dimethyl formamide then the metal salts $Co(NO_3)_2$. $6H_2O$ (2 mmol), $Cu(NO_3)_2.4H_2O$ (0.5 mmol), and $Ni(NO_3)_2.6H_2O$ (0.5 mmol) were added. This precursor was added to a Teflon-lined

stainless steel vessel that was kept at 160 °C for 12 h. Then, the product was cooled, separated, washed, dried, and stored for further use.

2.3. Synthesis of Zeolite/MOF Composite

In total, 2 g of the natural zeolite were suspended in 20 mL ethanol for 24 h under continuous stirring. A suspension of 0.25 g of the MOF in 50 mL ethanol was then added dropwise on zeolite and was left under stirring for 24 h. The formed nanocomposite was separated, washed several times with distilled water, and dried at 60 °C for 12 h.

2.4. Characterization

Both adsorbents were characterized using a PANalytical (Empyrean, Malvern Panalytical Ltd., Malvern, UK) X-ray diffractometer with Cu-Kα radiation from two-theta of 5° to 80° to determine the crystallinity of the sample. In addition, the functional groups before and after adsorption were determined using Fourier transform infrared (FTIR) spectroscopy (Bruker-Vertex 70, Bruker, Ettlingen, Germany) from a 400 to 4000 cm^{-1} wavenumber. The morphology of the ore was investigated using a field emission scanning electron microscope (Gemini Zeiss-Sigma 500 VP, Jena, Germany). Textural properties of the prepared material were investigated at 77 K by the N_2 adsorption–desorption isotherms using a Micromeritics ASAP 2010 device. The zeta potential investigation was conducted using a Zetasizer Nano instrument (Zeta-Meter Plus 3.0 equipment, Malvern Panalytical Ltd., Malvern, UK). Samples of both materials were suspended in 1 mL of water, ultrasonicated for 30 min, and measured in disposable folded capillary cells provided by the manufacturer.

2.5. Adsorption Experiments

Typically, 0.1 g of the adsorbents (zeolite, zeolite/MOF) was added to 20 mL of adsorbate solution, changing the adsorbate concentrations from 20 to 1000 mg/L for safinamide and from 3 to 20 mg/L for Cd^{2+}. The mixture was stirred for 2 h at 25 °C. By adding either 0.10 mol/L HCl or 0.10 mol/L NaOH solution, the initial pH of the solution was changed to values between 3 and 9, and the kinetic study was performed using 20 mg/L for each pollutant investigated. After centrifuging and separating the sample, an atomic absorption spectrophotometer and a UV-visible spectrophotometer were used to measure Cd^{2+} and safinamide concentrations, respectively. Calibration curves for safinamide detection are provided in the Supporting Information (Figure S1). The following formulas [45,46] were used to calculate the adsorption percentage and the adsorption capacity q_e (mg/g):

$$\text{adsorption percentage} = \frac{C_o - C_e}{C_o} \times 100 \quad (1)$$

$$q_e = \frac{(C_o - C_e) \times V}{m} \quad (2)$$

C_o and C_e are the initial adsorbate concentration and the equilibrium concentration, respectively (mg/L), m is the mass of the adsorbent, and V is the volume of the solution (L) [47].

For adsorption isotherm experiments, the Langmuir and Freundlich isotherm models were investigated to fit the experimental results for both Cd^{2+} and safinamide. The details of these models are illustrated in Table S1. Finally, safinamide and Cd^{2+} ion adsorption kinetics were investigated and then fitted to various kinetic models (Table S2).

The examined experiments were repeated more than 5 times.

2.6. Effect of Temperature

In ideal circumstances, the impact of temperature on the adsorption process was examined. Each flask holding 20 ppm of Cd^{2+} at 25, 35, 45, and 55 °C received 0.1 g of zeolite/MOF at pH 9. For 120 min, the flasks were shaken at various temperatures. After

filtering the zeolite/MOF out of the cd solution, an atomic absorption spectrophotometer was used to measure the cd concentration.

2.7. Regeneration Experiments

For adsorbent recovery investigations, desorbents such as acetone, ethanol, methanol, isopropanol, dimethylsulfoxide, dimethylformamide, and acetonitrile were utilized. Following the adsorption process, ten milligrams of adsorbent were combined with twenty milliliters of desorbent reagent. The samples were then agitated at 25 °C and 120 rpm for 24 h. The regeneration efficiency was determined using ultraviolet-visible spectrophotometry to quantify safinamide. Five regeneration cycles were implemented in adsorbent reuse experiments.

2.8. Real Sample Investigation

Zeolite/MOF was used at the optimum adsorption conditions to treat three real water samples (tap water, Nile River water, and groundwater) by spiking the collected samples with 20 ppm of safinamide.

2.9. Cytotoxicity Study

The potential cytotoxicity of the materials was evaluated in Vero cells using the MTT assay. Vero cells derived from the kidney of an African green monkey (ATCC CCL-81) were cultured in DMEM at a density of 5×10^4 cells/mL. The cells were seeded in 96-well plates and incubated for 24 h at 37 °C and 5% CO_2. After 24 h and 48 h, the medium was removed, and the cells were treated with varying concentrations of zeolite and zeolite/MOF samples (6.25, 12.5, 25, 50, 100, and 200 µg/mL) diluted in PBS. Each concentration was performed in triplicate. Some wells contained only solvent as a negative control. After 4 h and 48 h incubation at 37 °C and 5% CO_2, 10 µL of MTT reagent were added. Once orange formazan developed, absorbance was measured at 595 nm using an ELISA reader. The percentage of viable cells was calculated using Equation (3).

$$\text{Cell viability (\%)} = \text{absorbance of treatment} - \text{absorbance of Control media}/\text{absorbance of control of cells} - \text{absorbance of Control media} \times 100\%. \quad (3)$$

3. Results and Discussion

3.1. Characterization of Adsorbents

The crystal structure of the pure zeolite, pure Cu/Ni/Co ABDC (MOF), and zeolite/MOF samples were determined using the XRD test. As seen in Figure 1, the zeolite sample displayed clear, high-intensity XRD patterns that indicate the sample is crystalline. Based on the JCPDS Card No 00-025-1349, zeolite material showed the Clinoptilolite type indexed to 020, 200, 001, −220, 113, −131, 400, −222, −422, 151, and −621 at the 2θ = 9.9°, 11.3°, 13.1°, 15.2°, 17.3°, 19.13°, 22.1°, 26.3°, 28.2°, 30.1°, and 32.06°, respectively [30,31]. The XRD patterns for the MOF sample were 2θ = 9.2, 11.2, 14.3, 16.7, 17.8, 21.01, 24.3, 26.2, 43.4, and 44.7, which corresponded to (110), (220), (020), (333), (211), (202), (222), (040), (200), and (111), according to existing literature [48–50]. The presence of copper nanoparticles was confirmed by 2θ = 16.7 and 43.4 indices to the 020 and 200 planes, respectively [47,49]. 2θ = 44.7 (111) also confirmed the presence of nickel nanoparticles. Finally, cobalt was validated using the JCPDS Card No 00-018-0424 [50]. The XRD patterns revealed the zeolite patterns with more intensity for the zeolite/MOF. There was a definite overlap in the 110 and 220 planes for MOF and 020 and 200 planes for zeolite, which may explain why there are no MOF peaks in the zeolite/MOF spectrum.

The crystallite size of the zeolite and zeolite/MOF was computed depending on the Debye–Scherrer equation (Equation (4)) [49,51].

$$D = K\lambda/(\beta \text{Cos}\theta) \quad (4)$$

where K is a constant equal to 0.9, λ is the X-ray wavelength (Cu Kα = 0.15405 nm), β is the full width at half maximum, and θ is the Bragg's angle. Zeolite and zeolite/MOF were calculated to have crystallite sizes of 3.07 nm and 17.4 nm, respectively. The higher crystallite size of zeolite/MOF compared to pure zeolite indicates the deposition of MOF particles into zeolite layers.

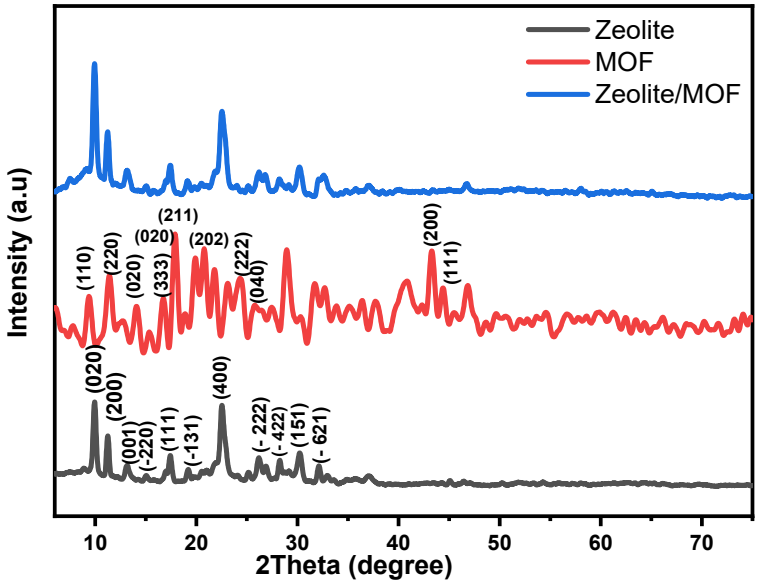

Figure 1. XRD patterns of pure Cu/Ni/Co ABDC (MOF) and Zeolite/MOF samples.

As shown in Figure 2, FT-IR spectra were used to evaluate and study the chemical structure of the generated materials. FTIR for zeolite, MOF, and zeolite/MOF samples are shown in Figure 2a. The water vapor molecules adsorbed on the surface and within pores of the zeolite matrix can be detected due to the stretching vibration of hydroxyl (-OH) groups evident from the broad peak at 3600–3300 cm^{-1} [52] and at 1700–1595 cm^{-1} [53]. The unique functional groups in zeolites, such as Si–O stretching vibrations, indicate their tetrahedral silicon–oxygen structure and are found in the 1100–1000 cm^{-1} range [54]. The band at 1058 cm^{-1} originates from the Si–O–Si bond [55]. Within the zeolite lattice, the stretching vibrations of the Al–O bonds are found at 800–750 cm^{-1}, Si–O–Si bends are seen at 650–600 cm^{-1}, and a band between 450 and 500 cm^{-1} is attributed to Si–O–Al [54,56,57].

As for the MOF sample, OH-related bands similar to those of the zeolite sample could be observed due to the presence of adsorbed water molecules. In addition, the broad band at approximately 3400 cm^{-1} originate from the asymmetric stretching mode of the N–H bond [58]. The peaks at 1550 cm^{-1} and 1392 cm^{-1} can be assigned to the asymmetrical and symmetrical stretching modes of the carboxylate groups [58]. The band at 1230 cm^{-1} may be assigned to C–N stretching vibrations [59]. Bands at 1052 cm^{-1} and 774 cm^{-1} can be attributed to the stretching vibration of the benzene ring, while the band around 673 cm^{-1} can be attributed to the COO bond [60]. Finally, the band at approximately 557 cm^{-1} can be attributed to metal–oxygen–hydrogen bending vibration (Ni–OH, Co–OH, and Cu–OH) [48]. The band at 897 cm^{-1} can be assigned to the carboxylic group [61]. For zeolite/MOF, the peaks originating from the zeolite phase were dominant in the spectra owing to the low loading of the MOF phase in the composite. A stronger indication of a chemical link between the MOF and zeolite could come from the increased strength of the OH and hydrogen interaction bands at 3600–3300 cm^{-1} and 1700–1595 cm^{-1}.

Figure 2b shows the FTIR spectra of spent adsorbent after adsorption. As shown, safinamide has numerous FTIR bands originating from functional groups in its structure. After adsorption, such bands were not clearly observed, probably due to their low loading and higher transmittance from bands originating from the adsorbent itself. After cadmium adsorption, no obvious change was also noticed for the FTIR of the spent adsorbent,

probably because of the ion exchange nature of zeolite for cadmium ions. Interaction between cadmium and OH groups in the zeolite structure may be pronounced in the increased intensity of low wavenumber peaks below 1000 cm^{-1}, which usually originate from metal–oxygen interaction.

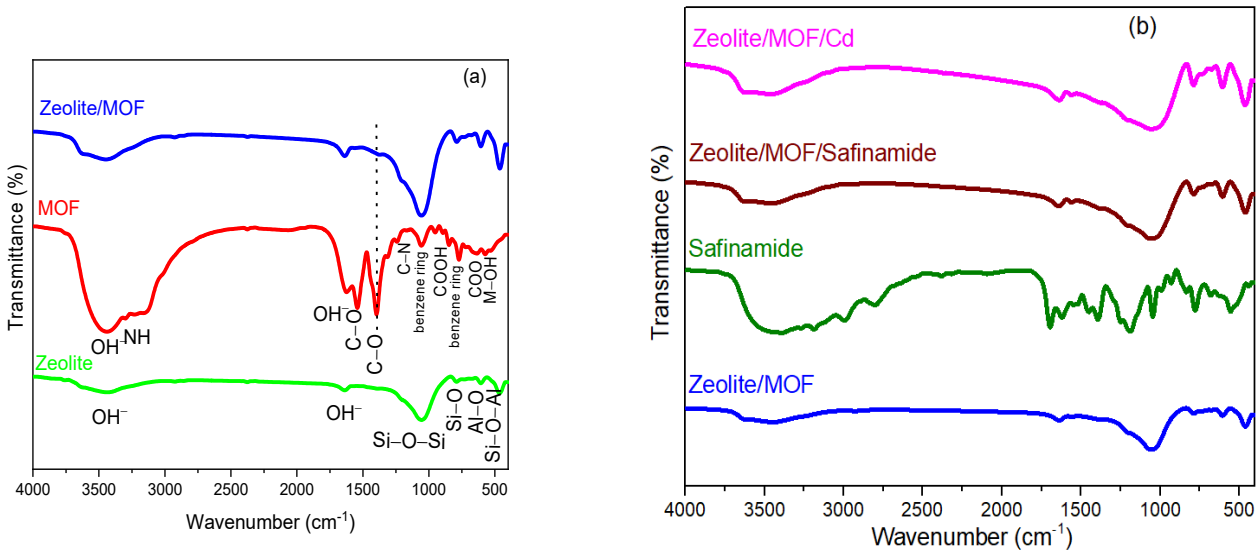

Figure 2. FTIR analysis of (**a**) zeolite, MOF, and zeolite/MOF. (**b**) Zeolite/MOF after safinamide adsorption (zeolite/MOF/Safinamide), and zeolite/MOF after cadmium adsorption (zeolite/MOF/Cd) samples.

The SEM morphology of zeolite (Figure 3a) showed a plate-like structure with a thickness of between 50 and 60 nm. The petal-like form indicates a high surface area suitable for the adsorption process. The MOF (Figure 3b) showed thick particles, ranging in size from 400 to 600 nm, with uneven, prismatic-edged forms. The nanocomposite zeolite/MOF (Figure 3c) showed the petal-like structures of the zeolite particles with a homogenous prismatic shape, indicating the formation of MOF within zeolite structures. To acquire elemental variations of surface features, qualitative EDX analysis and SEM study were combined for zeolite and zeolite/MOF, as depicted in Figures 3d and 3e, respectively.

The SEM image of the resulting composite, which can be seen in Figure 3f,g, has verified that the adsorbate has successfully adhered to the composite material by occupying the well-defined spaces and pores that have emerged in the SEM image of the prepared adsorbent, which displays a compact homogenous structure. Additionally, as seen in image (f), the skeleton has collapsed, the material surface is no longer tightly bound, and a significant number of amorphous particles, the majority of which may be adsorbed Cd^{2+} metal ions, have attached themselves to the material surface following the adsorption reaction.

The surface of the zeolite, Figure 3d, comprises O, Al, and Si with atomic ratios of 75.77%, 5.32%, and 18.9%, respectively. Figure 3e shows the elemental surface study of zeolite/MOF, which contains the main metals of MOF and zeolite. O, Al, Si, Co, Ni, and Cu elements have atomic ratios of 78.73%, 4.48%, 16.3%, 0.21%, 0.07%, and 0.01%, respectively. The absence of other foreign elements reflects the purity of the synthesized zeolite/MOF sample.

The textural characteristics of the zeolite and zeolite/MOF material, such as specific surface area, pore volume, and pore size, were distributed using the N_2 adsorption–desorption technique in Figure 3g,h. The two materials estimated an isotherm type of IV and a hysteresis loop type of H3 [62]. H3 type is related to a broad range of non-uniformly sized slit-shaped pores that appear in solids [63]. The specific surface area, pore volume, and average pore size of zeolite/MOF are all greater than those of pure zeolite, as shown in Table 2. These results significantly promote the formation of a Zeolite/MOF composite.

Figure 3i displays the pore size distribution estimated from the nitrogen desorption branch of the isotherm. Notably, the Zeolite/MOF sample demonstrated the narrowest pore size.

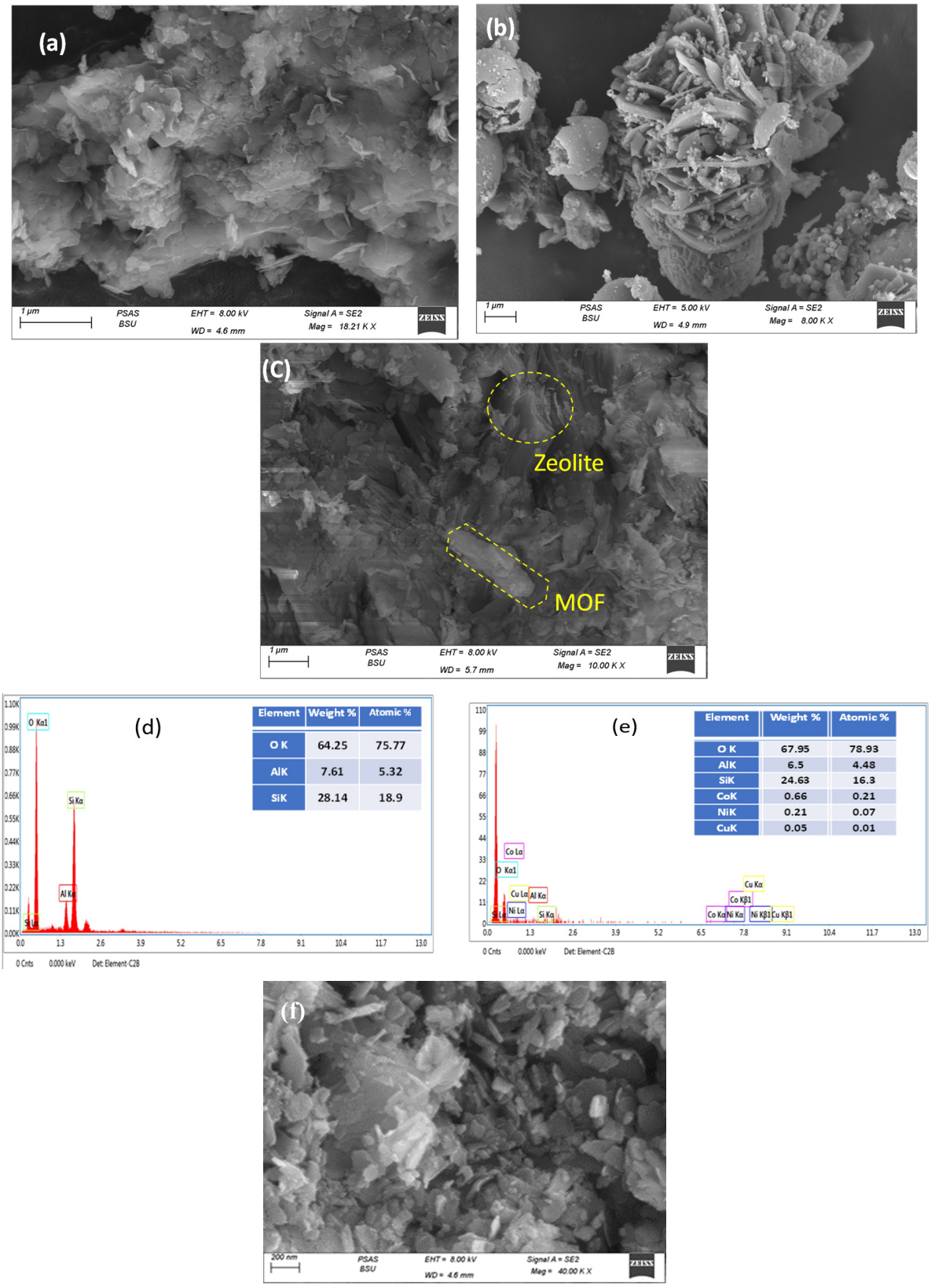

Figure 3. *Cont.*

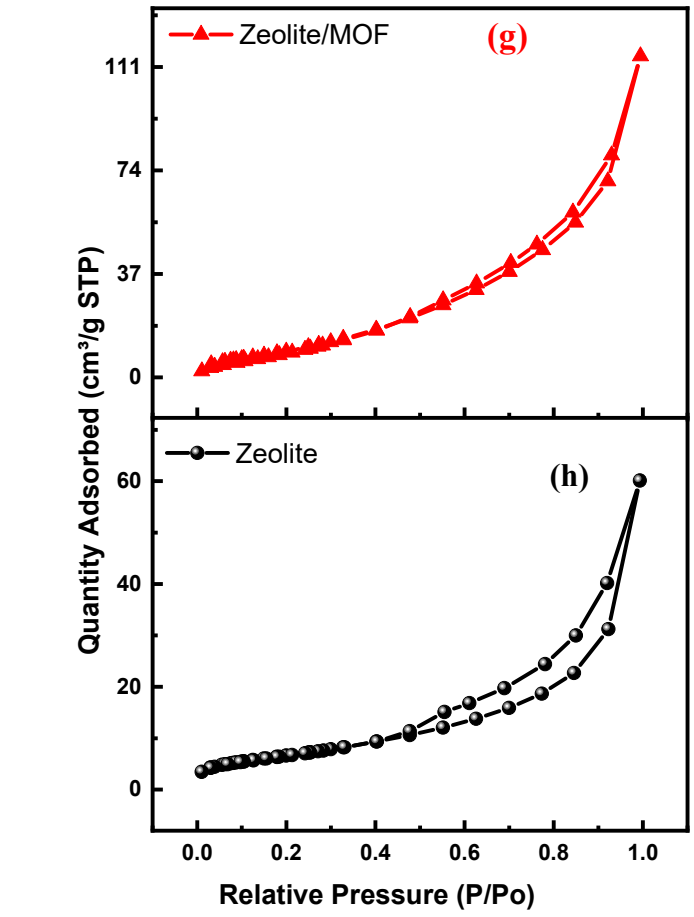

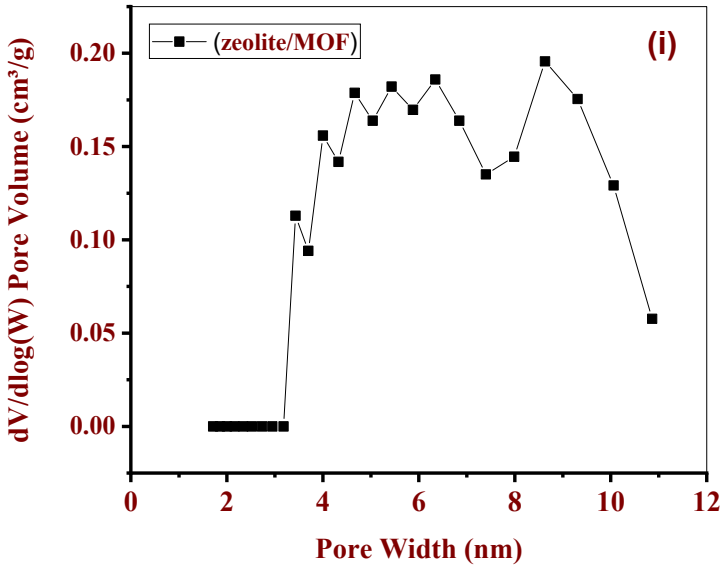

Figure 3. SEM micrographs of (**a**) zeolite, (**b**) pure MOF, and (**c**) Zeolite/MOF samples. (**d**,**e**) EDX analysis of zeolite and zeolite/MOF samples, respectively, (**f**) for the Zeolite/MOF sample after Cd^{2+} adsorption, N_2 adsorption–desorption isotherms of (**g**) Zeolite, (**h**) Zeolite/MOF samples and (**i**) pore size distribution of Zeolite/MOF.

Table 2. Specific surface, pore volume, and average pore size of zeolite and zeolite/MOF samples.

Nanomaterial	Surface Area (m^2/g)	Pore Volume ($cm^3\ g^{-1}$)	Pore Size (nm)
zeolite	24.63	0.091	14.7
zeolite/MOF	41.86	0.173	16.5

Zeta potential experiments demonstrate the stability of the synthesized zeolite/MOF material. They assess how strongly electrically charged particles in a solution will either attract or repel one another. Zeolite/MOF material zeta potential measurements, which were −27.9 mV, demonstrate the produced nanoparticles' great degree of stability. Figure 4a shows the zeta potential, and Figure 4b shows the size distribution of zeolite/MOF material. Figure 4c,d demonstrate the zeta potentials of zeolite and MOF samples, respectively. The Zeolite/MOF size was 730.4 nm. The zeta potentials for zeolite and MOF samples were calculated to be −18.6 mV and −12.6 mV, as shown in Figure 4.

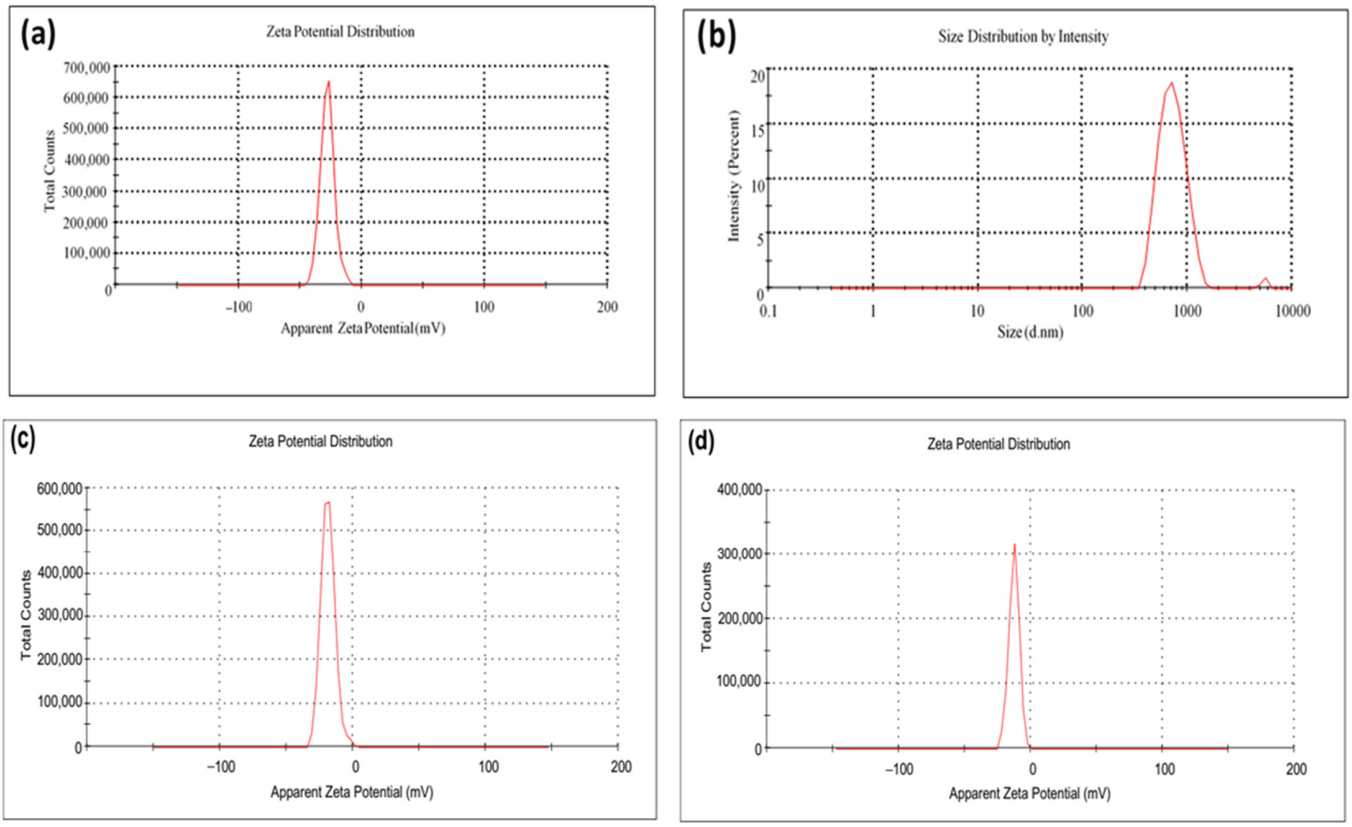

Figure 4. (**a**) zeta potential and (**b**) Size distribution of zeolite/MOF material. (**c**,**d**) are the zeta potentials of zeolite and MOF samples, respectively.

3.2. Adsorption Study

3.2.1. Effect of pH

The elimination of contaminants from water is significantly affected by pH. Its effect on the removal process is caused by the charge it provides to the pollutants and adsorbents. Safinamide has a pKa of 7.4 [64]. At pH < 7.4, safinamide is primarily cationic, while at pH > 7.4, the anionic form is the major species. Also, the point of zero charge of zeolite and zeolite/MOF calculated by the pH drift method is 6.9 and 7.01, respectively. When the pH of safinamide solution > pHpzc of two adsorbents, the surface charges will be positive, while at pH < pH pzc, the charge will be negative. The effect of pH on the adsorption of safinamide and Cd^{2+} (Figures 2b and 5A) shows a maximum adsorption percentage of 48.8% for safinamide at pH 5 for both adsorbents. Then, the adsorption percentage

decreases at pH > 5, demonstrating that the alkaline environment fails to improve the adsorption of safinamide on two adsorbents. Consequently, this decline in safinamide adsorption above pH 5 may be attributed to the decreased electrostatic attraction between safinamide molecules and zeolite, as well as zeolite and MOF, which possess negatively charged surfaces and the competition between OH groups and the negatively charged safinamide molecule. As presented in Figure 5, showing the effect of pH on the adsorption percentage of (A) safinamide and (B) Cd^{2+} onto zeolite and zeolite/MOF.B, the adsorption of Cd^{2+} ions onto zeolite and zeolite/MOF is high with increasing pH. The maximum adsorption percentage of Cd ions (48.9%) by zeolite was observed at a pH of 7. In contrast, the percentage of Cd adsorbed onto zeolite/MOF increased from 27.8% to 80% with increasing pH from 3 to 9. The relatively low Cd adsorption at low pH may be related to the structural alteration of zeolite in acidic environments and the competition for active binding sites on the adsorbent between H^+ and Cd^{2+} ions [65,66]. When the pH is high (7–9), the concentration of hydrogen ions decreases, thereby increasing the availability of active binding sites for cadmium ions.

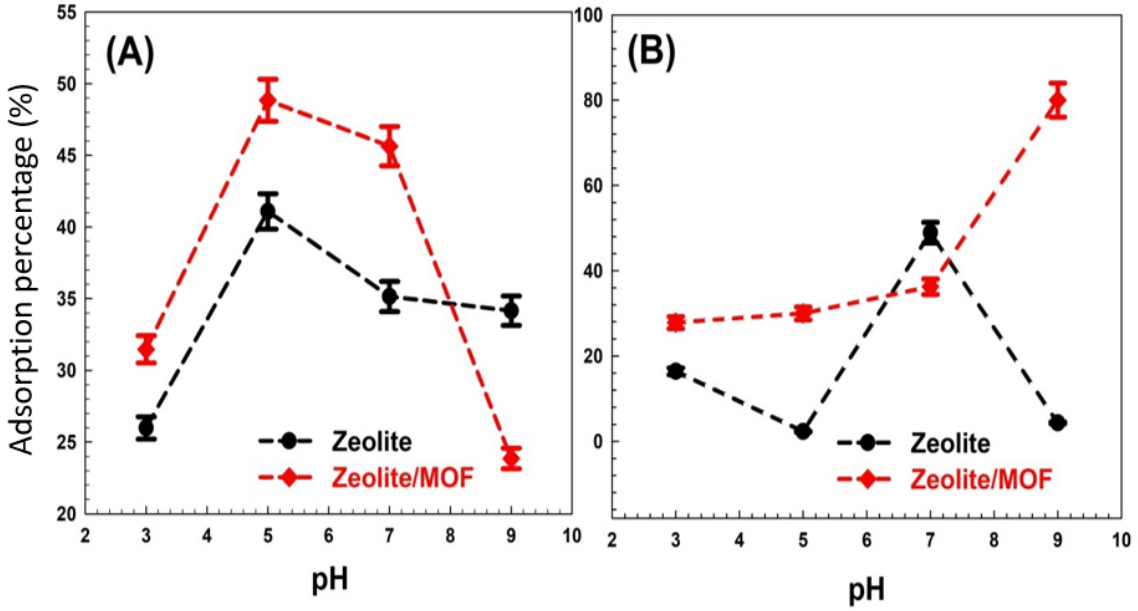

Figure 5. Effect of pH on the adsorption percentage of (**A**) safinamide and (**B**) Cd^{2+} onto zeolite and zeolite/MOF.

3.2.2. Effect of Adsorbent Dose

The dosage of the adsorbent is a critical variable that significantly influences the adsorption procedure. Figure 6A shows the adsorption of safinamide onto zeolite and zeolite/MOF. The drug adsorption percentage rose with the increase in the amount of zeolite until the maximum value reached 0.15 g. Beyond this value, the adsorption percentage stabilized. Meanwhile, for zeolite/MOF, the amount of the absorbed drug rose with the increasing amount of zeolite/MOF until the maximum was reached at 0.1 g/L. Figure 6B depicts the effect of zeolite and zeolite/MOF dosage on the removal of Cd^{2+}. The removal efficiency of Cd^{2+} reached 97.19% for a 0.1 g adsorbent dose of zeolite. On the other hand, over the range of investigated dosages, the zeolite/MOF adsorbent showed a maximum adsorption percentage of 99.9%.

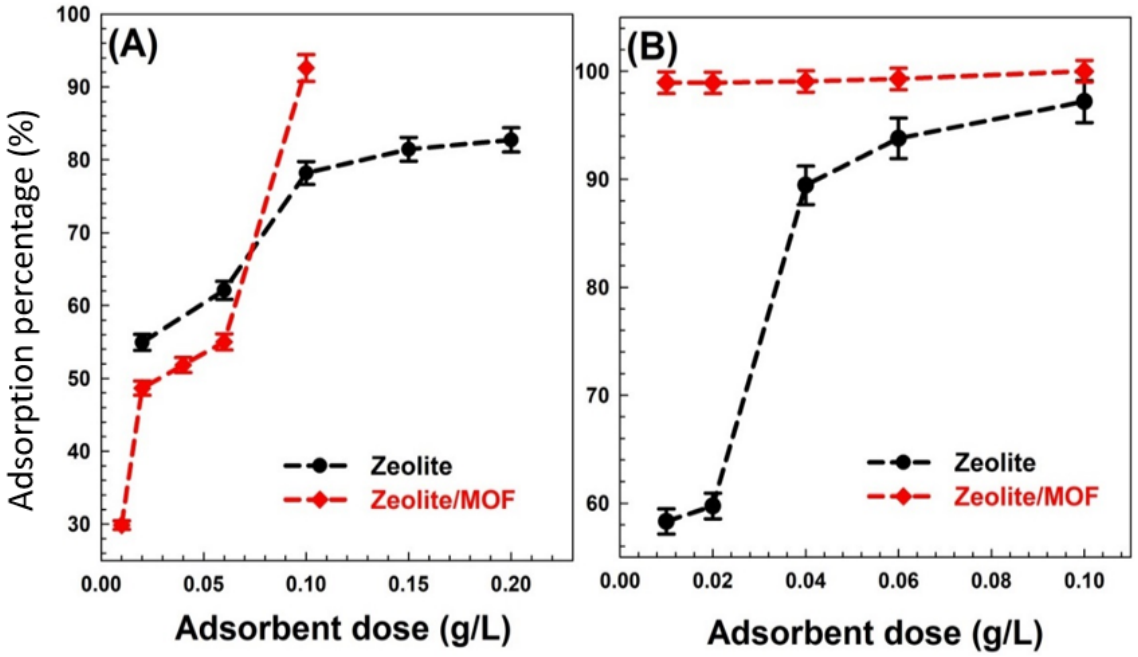

Figure 6. Effect of adsorbent dose on the adsorption of (**A**) safinamide and (**B**) Cd (II) onto zeolite and zeolite/MOF.

3.2.3. Adsorption Isotherm

An adsorption isotherm is used to establish a relation between adsorption equilibrium and the initial concentration of adsorbate [67]. Several adsorption isotherms can be used to evaluate the adsorbate distribution between the liquid and solid phases once the adsorbent uptake has reached equilibrium. The amount of adsorbate per unit mass of the adsorbent as a function of concentration at constant pH and temperature is represented by fitting the data to the adsorption isotherm model. It can be used to describe how materials are adsorbed onto the surface of the adsorbent and determine the maximum adsorption capacity of drug residue or Cd^{2+} metal ions. The Langmuir and Freundlich models were investigated in this work to explain adsorption isotherms.

The Langmuir model for the two-parameter models postulates that adsorption occurs at particular, similar adsorption sites localized on the catalyst surface, coating it with a monolayer of the adsorbate. The Freundlich isotherm model describes the multilayer adsorption of adsorbed molecules onto a heterogeneous adsorbent surface. To compare which isotherm equations match the data the most exactly, the highest determination coefficient, R^2, is employed. The R^2 values and all other characteristics for each isotherm are compared in Tables S3 and S4 for safinamide and Cd metal ion adsorption, respectively. According to the calculated coefficients (R^2) in Table 3, the adsorption data suited Langmuir isotherm models (Figure 7a) most effectively for the adsorption of safinamide onto zeolite and zeolite/MOF (Figure 7b). This can reflect that the adsorption of safinamide on both adsorbents was monolayer adsorption. For cadmium adsorption, the best model to fit the experimental data on the zeolite support was the Freundlich isotherm model (Figure 7c), which reflects a heterogeneous adsorption nature with multilayer adsorption. On the other hand, when the nanocomposite was used, the Langmuir model (Figure 7d) showed the highest R^2 value (Table 3), Table 4 which reflects monolayer adsorption for Cd metal ions. The statistical error validity statistics for the isotherm models are shown in Tables 5–8. It has been noted that the values of various statistical techniques increase with model quality and decrease with the degree of agreement between the experimental quantity adsorbed (qe, exp) and the calculated quantity adsorbed (qe, cal). The coefficient of regression (R^2) was mentioned to help the comparison of the best model. R^2 values that are higher and tighter are qe, exp, and qe, cal values.

Table 3. Adsorption isotherm fitting parameters for safinamide adsorption onto zeolite and zeolite/MOF.

Isotherm Models	Parameter	Value	
		Zeolite	Zeolite/MOF
Langmuir	Q_{max} (mg/g)	88.91	500.69
	K_L (L/mg)	0.003	0.00042
	R^2	0.998	0.999
Freundlich	1/n	0.79	0.79
	K_F	0.52	0.52
	R^2	0.994	0.992
Redlich–Peterson	K_R	0.75	0.3
	a_R	0.007	0.0017
	R^2	0.887	0.985
Temkin	A_T (L/mg)	2.612330	1.612330
	b_T	390.6960	600.6960
	R^2	0.715	0.858
Sips	q_m (mg/g)	64.03	23.76
	Ks	0.006	0.01
	1/n	1.01	1.24
	R^2	0.978	0.928
Langmuir–Freundlich	*q*MLF (mg/g)	62.19	19.32
	*K*LF (L/mg)	0.0063	0.027
	*M*LF	1.13	6
	R^2	0.999	0.956
Toth	K_e	0.5	0.55
	K_L	0.00001	0.007
	N	2.3	1.2
	R^2	0.999	0.899
Kahn	Q_m (mg/g)	34.32	31.11
	b_K	0.006	0.006
	a_K	0.32	0.18
	R^2	0.986	0.985
Fritz–Schlunder	q_{mFSS} (mg/g)	19.17	55.19
	K_1	0.67	0.04
	K_2	3.29	0.79
	m_1	0.47	0.58
	m_2	0.00006	0
	R^2	0.936	0.952

Table 4. Adsorption isotherm fitting parameters for Cd (II) adsorption onto zeolite and zeolite/MOF.

Isotherm Models	Parameter	Value	
		Zeolite	Zeolite/MOF
Langmuir	Q_{max} (mg/g)	500.69	550.69
	K_L (L/mg)	0.0021	0.0021
	R^2	0.970	0.962
Freundlich	1/n	0.67	1.49
	K_F	1.43	0.71
	R^2	0.987	0.923
Temkin	A_T (L/mg)	1.15	1.05
	b_T	4.31	4.15
	R^2	0.981	0.646

Table 4. *Cont.*

Isotherm Models	Parameter	Value	
		Zeolite	**Zeolite/MOF**
Redlich–Peterson	K_R	0.91	1.18
	a_R	0.00001	0.0000001
	R^2	0.822	0.847
Langmuir–Freundlich	*q*MLF (mg/g)	5.52	34.47
	*K*LF (L/mg)	0.39	0.089
	*M*LF	1.09	1.61
	R^2	0.999	0.922
Sips	q_m (mg/g)	5.52	42.5
	K_s	0.37	0.02
	1/n	1.09	1.6
	R^2	0.999	0.923
Toth	K_e	2.22	8.5
	K_L	0.17	0.00012
	N	1.3	7.3
	R^2	0.999	0.852
Kahn	Q_m (mg/g)	180.1	79.1
	b_K	0.006	0.014
	a_K	0.29	0
	R^2	0.986	0.875
Fritz–Schlunder	q_{mFSS} (mg/g)	13.9	9.84
	K_1	0.11	0.077
	K_2	0.068	0.068
	m_1	0.67	1.49
	m_2	00.93	0
	R^2	0.987	0.923

Table 5. Summary of the determined error functions for the non-linear adsorption isotherm models for safinamide adsorption onto zeolite.

Function	Lang	Fran	Lan-Fru	Toth	Sips	Baudu
SSE/ERRSQ	10.79858	11.1424	15.76554	2.280182	2428.948	120.6874
X2	0.729908	2.394497	1.41119	0.116225	72.10261	5.226423
R^2	0.996188	0.995554	0.993709	0.999195	0.030706	0.9574
Adjusted R^2	0.989855	0.987578	0.978049	0.997426	−0.74835	0.83323
MAE	0.810396	1.019874	0.870645	0.380207	12.64043	2.652084
MAPE/ARE	15.80149	52.83145	11.676	5.258558	48.56495	30.09969
RMSE	1.095373	1.18017	1.403814	0.503342	17.42465	3.661927
RMSE_2	1.242036	1.362742	1.775699	0.616466	22.04064	4.912991
NRMSE	0.07872	0.107368	0.127715	0.036173	1.585245	0.263167
HYBRID	20.3162	70.44194	18.6816	7.887836	77.70393	54.17944
HYBRID_2	10.42725	39.90828	28.22381	1.937082	1442.052	104.5285
HYBRID_3	0.729908	2.394497	1.41119	0.116225	72.10261	5.226423
MPSD	25.10817	95.37887	21.69583	8.622271	70.97156	49.45509
MPSD_2	0.441294	5.458277	0.235355	0.044606	2.518481	1.222903
SAE/EABS	7.293566	8.15899	6.965158	3.421867	101.1235	23.86876
RMS	22.14333	82.60052	17.15206	7.040055	56.10795	36.86164
NSD	0.221433	0.826005	0.171521	0.070401	0.561079	0.368616
ARE_2	4.903269	68.22847	2.941933	0.495624	31.48102	13.58781
ARE_3	7.381109	29.2037	6.06417	2.346685	19.83716	12.28721

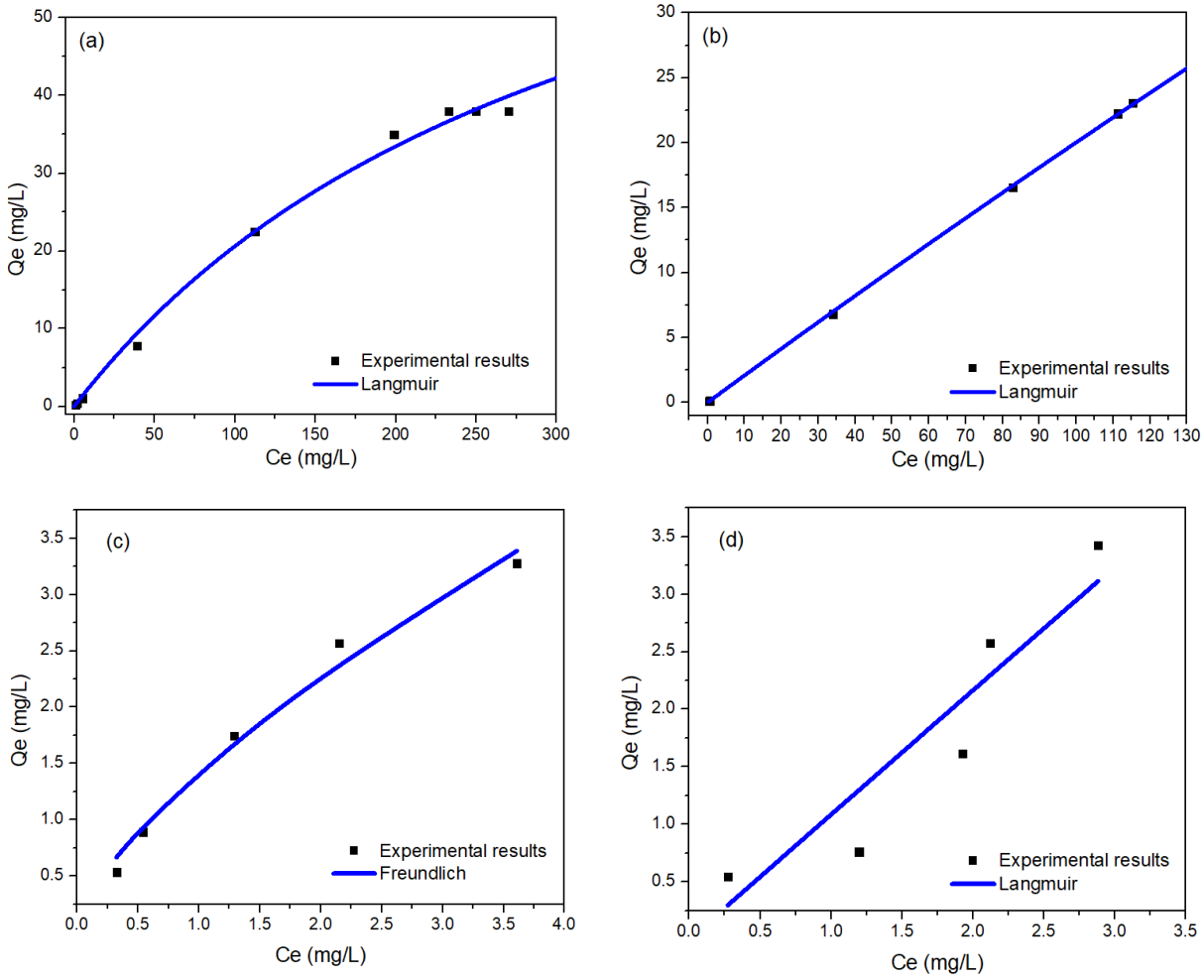

Figure 7. Best fit isotherm model for safinamide adsorption onto (**a**) zeolite and (**b**) zeolite/MOF; best-fit isotherm model for Cd^{2+} adsorption onto (**c**) zeolite and (**d**) zeolite/MOF.

Table 6. Summary of the determined error functions for the non-linear adsorption isotherm models for safinamide adsorption onto zeolite/MOF.

Function	Lang	Fran	Lan-Fru	Sips	Khan	Baudu	Toth
SSE/ERRSQ	0.073115	5.544945	0.023627	0.02859	10.00939	0.002155	0.003454
X2	0.008005	1.640773	0.021021	0.024026	0.470037	0.002722	0.000346
R^2	0.99991	0.993175	0.999971	0.999965	0.987679	0.999997	0.999996
Adjusted R^2	0.99973	0.979594	0.999884	0.999859	0.95102	0.999984	0.999983
MAE	0.073833	0.677543	0.049058	0.052634	0.792977	0.014302	0.015911
MAPE/ARE	2.485364	92.30731	11.54097	12.32377	4.118834	4.164361	0.838876
RMSE	0.102201	0.89002	0.058097	0.063908	1.195789	0.017545	0.022214
RMSE_2	0.120926	1.053085	0.076856	0.084542	1.581881	0.026801	0.029387
NRMSE	0.019267	0.167784	0.010952	0.012048	0.225427	0.003308	0.004188
HYBRID	3.47951	129.2302	20.1967	21.5666	7.207959	9.716842	1.468033
HYBRID_2	0.160104	32.81547	0.525521	0.600651	11.75092	0.090731	0.00864
HYBRID_3	0.008005	1.640773	0.021021	0.024026	0.470037	0.002722	0.000346
MPSD	3.606687	158.6748	22.77803	24.33586	7.571163	9.513039	1.482882
MPSD_2	0.006504	12.58885	0.207535	0.236894	0.022929	0.027149	0.00088
SAE/EABS	0.516831	4.742802	0.343404	0.368441	5.550836	0.100114	0.111375
RMS	3.048207	134.1047	17.21857	18.39618	5.723261	6.227746	1.120953
NSD	0.030482	1.341047	0.172186	0.183962	0.057233	0.062277	0.01121
ARE_2	0.092916	179.8407	2.964791	3.384194	0.327557	0.387848	0.012565
ARE_3	1.152114	50.68681	6.508007	6.953102	2.163189	2.353867	0.42368

Table 7. Summary of the determined error functions for the non-linear adsorption isotherm models for the adsorption of Cd^{2+} onto zeolite.

Function	Lang	Fran	Lan-fru	Sips	Khan	Baudu	Toth
SSE/ERRSQ	0.631032	0.066719	0.005373	0.005373	0.023602	0.007703	0.004007
X2	0.401996	0.053206	0.002827	0.002826	0.021668	0.004508	0.002607
R^2	0.944472	0.994129	0.999527	0.999527	0.997923	0.999322	0.999647
Adjusted R^2	0.784055	0.976585	0.996219	0.996219	0.983403	0.994579	0.99718
MAE	0.345894	0.10486	0.026754	0.026736	0.05676	0.03204	0.023335
MAPE/ARE	25.07276	8.765816	1.560858	1.55893	5.491793	2.2793	1.605197
RMSE	0.355256	0.115516	0.032781	0.032781	0.068704	0.03925	0.028308
RMSE_2	0.458633	0.14913	0.051831	0.051831	0.108631	0.06206	0.044759
NRMSE	0.512145	0.16653	0.047258	0.047258	0.099046	0.056584	0.04081
HYBRID	41.78793	14.60969	3.902146	3.897326	13.72948	5.698251	4.012993
HYBRID_2	13.39987	1.773532	0.141374	0.141324	1.083419	0.225414	0.130363
HYBRID_3	0.401996	0.053206	0.002827	0.002826	0.021668	0.004508	0.002607
MPSD	35.21014	15.38348	2.90513	2.903674	11.742	4.605424	3.155022
MPSD_2	0.371926	0.070995	0.001688	0.001686	0.027575	0.004242	0.001991
SAE/EABS	1.72947	0.524301	0.133772	0.133678	0.283799	0.160201	0.116673
RMS	27.27366	11.916	1.837366	1.836445	7.426292	2.912726	1.995411
NSD	0.272737	0.11916	0.018374	0.018364	0.074263	0.029127	0.019954
ARE_2	7.438525	1.419909	0.033759	0.033725	0.551498	0.08484	0.039817
ARE_3	12.19715	5.328995	0.821695	0.821283	3.321139	1.302611	0.892375

Table 8. Summary of the determined error functions for the non-linear adsorption isotherm models for the adsorption of Cd^{2+} onto zeolite/MOF.

Function	Lang	Fran	Lan-Fru	Sips	Baudu
SSE/ERRSQ	0.748248	0.4551	0.458208	0.457622	0.455174
X2	0.68922	0.506278	0.522122	0.519105	0.506484
R^2	0.937409	0.961931	0.961671	0.96172	0.961925
Adjusted R^2	0.757472	0.850623	0.699245	0.699622	0.701197
MAE	0.369643	0.266439	0.263353	0.26411	0.266297
MAPE/ARE	33.05395	27.58417	27.57689	27.59684	27.57782
RMSE	0.386846	0.301695	0.302724	0.30253	0.30172
RMSE_2	0.499416	0.389487	0.478648	0.478342	0.477061
NRMSE	0.563751	0.439661	0.441159	0.440877	0.439696
HYBRID	55.08992	45.97362	68.94222	68.99209	68.94454
HYBRID_2	22.97401	16.87592	26.10608	25.95527	25.32418
HYBRID_3	0.68922	0.506278	0.522122	0.519105	0.506484
MPSD	52.01103	50.45494	63.20967	62.93608	61.81552
MPSD_2	0.811544	0.76371	0.799092	0.79219	0.764232
SAE/EABS	1.848213	1.332195	1.316763	1.320549	1.331485
RMS	40.28757	39.08223	39.9773	39.80427	39.09557
NSD	0.402876	0.390822	0.399773	0.398043	0.390956
ARE_2	16.23089	15.27421	15.98185	15.8438	15.28464
ARE_3	18.01715	17.47811	17.87839	17.80101	17.48407

The dimensionless constant, R_L (separation factor), can be calculated from the following equation [67]:

$$R_L = \frac{1}{1 + K_L C_o} \quad (5)$$

R_L values designate the adsorption as unfavorable when $R_L > 1$, linear when $R_L = 1$, favorable when $0 < R_L < 1$, and irreversible when $R_L = 0$. In this study, R_L for safinamide and Cd^{2+} adsorption on zeolite was calculated to be 0.25 and 0.7, respectively. As for zeolite/MOF, the values of R_L were 0.96 and 0.959 for safinamide and Cd^{2+}, respectively. These values indicate favorable adsorption of both adsorbates on both adsorbents. For Cd^{2+} adsorption on zeolite, the value of 1/n from the Freundlich model was less than one,

which indicates a favorable physisorption condition [68]. The Toth, Langmuir–freundlich, and Sips three-parameter models were also applied. In general, these models are useful for illustrating heterogeneous adsorption frameworks with both low and extremely good adsorbate quality limits [69]. The Langmuir–Freundlich isotherm model provides a signal concerning heterogeneous surfaces and the adsorption energy circulation on them [69]. A combination of the Langmuir and Freundlich isotherm models is the Sips isotherm model. This model minimizes the Freundlich model at low adsorbate concentrations but predicts the Langmuir model at high adsorbate concentrations [70]. By comparing other multicomponent adsorption isotherms, the Khan isotherm model has been utilized to describe the experimental data for the adsorption of various contaminants from aqueous solutions with the lowest average percentage error [71]. The Freundlich and Langmuir isotherms' components are combined to form the Redlich–Peterson isotherm model [72]. Due to the Fritz–Schunder three-parameter isotherm's huge number of coefficients, it was designed to accommodate a wide range of experimental results [73]. The highest determination coefficient, R^2, is used to compare which isotherm equations most closely match the data. The R^2 values and all other characteristics for each isotherm are compared in Table 3 for safinamide or Cd^{2+} adsorption [74,75].

3.2.4. Adsorption Kinetics Investigation

The ability to estimate the adsorption rate is important for the development of any adsorption system because it enables the selection of the optimal adsorption time. The following kinetic models were tested: pseudo first-order, pseudo second-order, intraparticle diffusion, mixed 1- and 2-order, and the Avrami model. The parameters for each model were determined and summarized in Tables 9 and 10 for safinamide and Cd adsorption, respectively. According to R^2 in Table 9, data were best fitted with intraparticle diffusion for the adsorption of safinamide onto zeolite (Figure 8a). The same model showed the highest R^2 value when zeolite/MOF was used (Figure 8b). The intraparticle diffusion model is one of the internal diffusion models that reflects that the adsorbate diffusion within the adsorbent is the slowest step [76]. This model shows that the intra-particle diffusion step is the rate-determining step [77]. The adequacy of this model can reflect the difficulty of safinamide diffusion due to its large size within the zeolite pores either before or after the addition of the MOF phase.

Table 9. The parameters of kinetic models for the adsorption of safinamide onto zeolite and zeolite/MOF.

Model	Parameters	Values	
		Zeolite	**Zeolite/MOF**
Pseudo first-order	K_1 (min^{-1})	0.02	8.06589×10^8
	q_e (mg/g)	0.29	0.82
	Adjusted R^2	0.76	0.74
	Reduced chi-square	0.002	0.02
	R^2	0.78	0.77
Pseudo second-order	K_2 (g/(mg min))	0.1	4.48995×10^{44}
	q_e (mg/g)	0.32	0.82
	Adjusted R^2	0.82	0.75
	Reduced chi-square	0.001	0.022
	R^2	0.84	0.77
Intraparticle diffusion	Kip	0.06	0.013
	Cip	0.017	0.0011
	R^2	0.983	0.994
	Reduced chi-square	0.001	0.01
	Adjusted R^2	0.981	0.993

Table 9. *Cont.*

Model	Parameters	Values	
		Zeolite	Zeolite/MOF
Mixed first- and second-order	K (g/(mg min))	0.0048	0.25
	qe (mg/g)	0.39	0.89
	f_2	0.098	0.03
	R^2	0.967	0.950
	Reduced chi-square	0.003	0.099
	Adjusted R^2	0.958	0.942
Avrami model	Kav (min^{-1})	0.012	0.23
	nav	1.43	0.23
	qe (mg/g)	0.29	0.88
	R^2	0.769	0.949
	Reduced chi-square	0.005	0.03
	Adjusted R^2	0.743	0.941

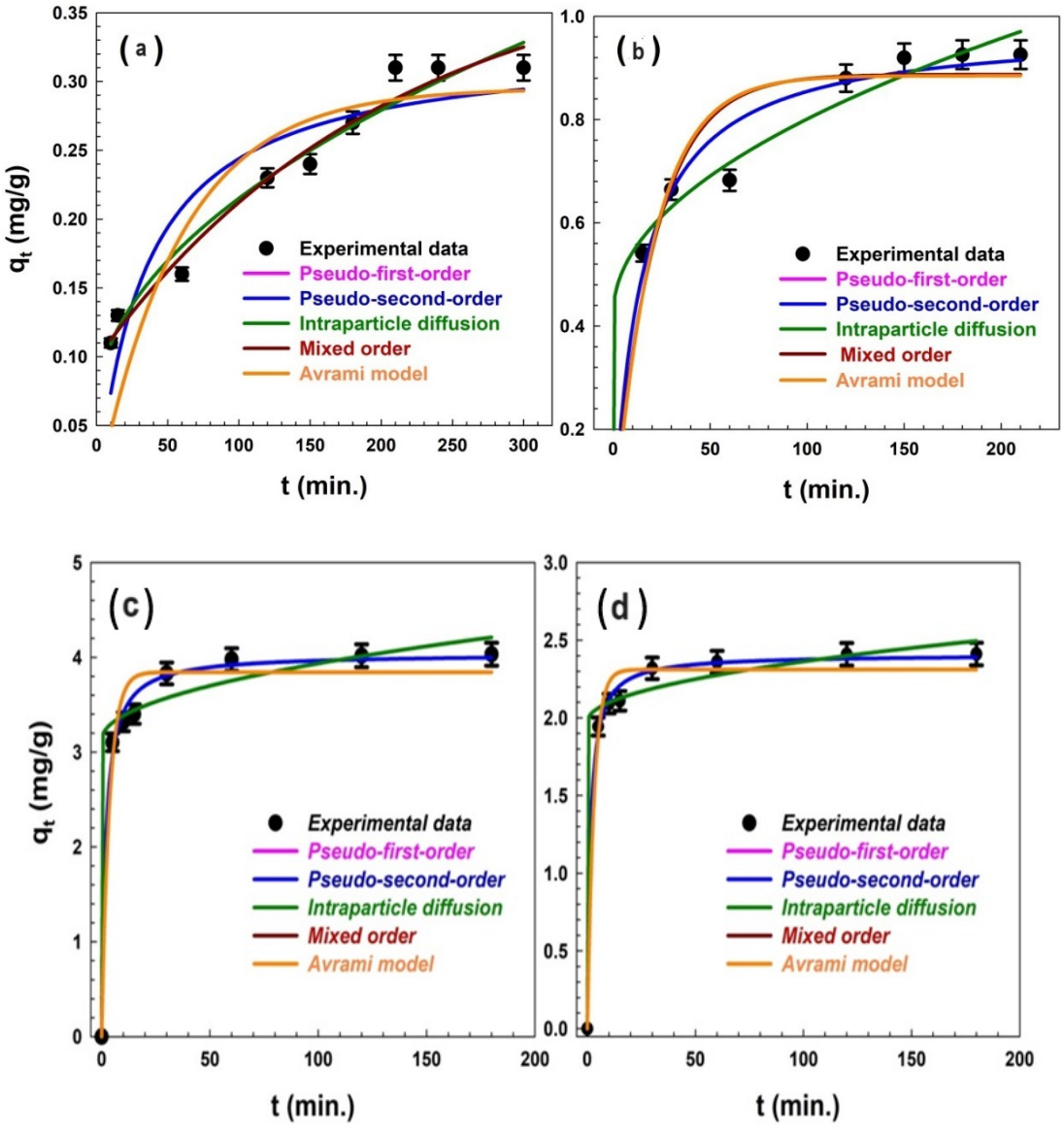

Figure 8. Kinetic model fitting for safinamide adsorption onto (**a**) zeolite and (**b**) zeolite/MOF; kinetic model fitting for Cd^{2+} adsorption onto (**c**) zeolite and (**d**) zeolite/MOF.

Table 10. The parameters of kinetic models for the adsorption of Cd onto zeolite and zeolite/MOF.

Model	Parameters	Values	
		Zeolite	**Zeolite/MOF**
Pseudo first-order	K_1 (min^{-1})	0.28 ± 0.05	2.23 ± 0.07
	q_e (mg/g)	3.84	1.04×10^{11}
	Adjusted R^2	0.97	0.95
	Reduced chi-square	0.06	0.034
	R^2	0.97	0.96
Pseudo second-order	K_2 (g/(mg min))	0.14	0.304 ± 0.04
	q_e (mg/g)	4.04	2.4 ± 0.03
	Adjusted R^2	0.993	0.99
	Reduced chi-square	0.012	0.0024
	R^2	0.994	0.99
Intraparticle diffusion	Kip	3.13	0.013
	Cip	0.08	0.001
	R^2	0.992	0.994
	Reduced chi-square	0.009	0.01
	Adjusted R^2	0.990	0.993
Mixed first- and second-order	K (g/(mg min))	0.0048	0.33
	q_e (mg/g)	0.39	2.31
	f_2	0.098	0.0064
	R^2	0.967	0.982
	Reduced chi-square	0.0001	0.00006
	Adjusted R^2	0.960	0.979
Avrami model	K_{av} (min^{-1})	0.012	0.29
	n_{av}	1.43	1.16
	q_e (mg/g)	0.29	2.31
	R^2	0.769	0.975
	Reduced chi-square	0.0005	0.0003
	Adjusted R^2	0.722	0.971

According to R^2 in Table 10, data were best fitted with a pseudo second-order model for the adsorption of Cd onto zeolite (Figure 8c), while adsorption information suited the intraparticle diffusion model for the adsorption of Cd onto zeolite/MOF (Figure 8d). The adequate fitting of the kinetic data to the pseudo second-order model can indicate that the zeolite support has abundant active sites that can adsorb Cd^{2+} easily and quickly, probably leading to a diffusion-limited adsorption process [76,78]. In other words, this model suggests that Cd^{2+} adsorption occurs at a very fast rate compared to the rate of diffusion of these ions from the bulk of solution to the active sites present on the zeolite surface within its pores. After MOF addition to the zeolite, it can be assumed that the MOF phase decreased the pore size of the zeolite support and increased the resistance of Cd^{2+} diffusion within the pores rather than from the bulk of the solution, leading to an internal diffusion limited adsorption process.

3.3. Desorption Study

Desorption and regeneration steps are required to investigate the applicability of a given adsorbent. If an adsorbent cannot be desorbed or regenerated effectively, the application value of the adsorbent is reduced and may create secondary environmental pollution. Therefore, the nanocomposite was regenerated using different solvents (methanol, ethanol, acetonitrile, isopropanol, acetone, dimethylformamide, and dimethylsulfoxide). As shown in Figure 9a, the desorption efficiency reached above 35.04% after 24 h using methanol, 29.51 using ethanol, and 2.17 using isopropanol. In addition, acetonitrile did not result in appreciable safinamide desorption, while acetone and dimethylformamide showed desorption efficiencies of 21.6% and 61.8%. The eluent showing the highest desorption efficiency

was dimethylsulfoxide, which reached 63.74%, probably due to the high solubility of safinamide in dimethylsulfoxide, which reached 30 mg/mL [79]. Reuse of the adsorbent was conducted in DMSO, as shown in Figure 9b, where almost no observable loss in removal efficiency was observed for three consecutive cycles, indicating the promising reusability of this adsorbent.

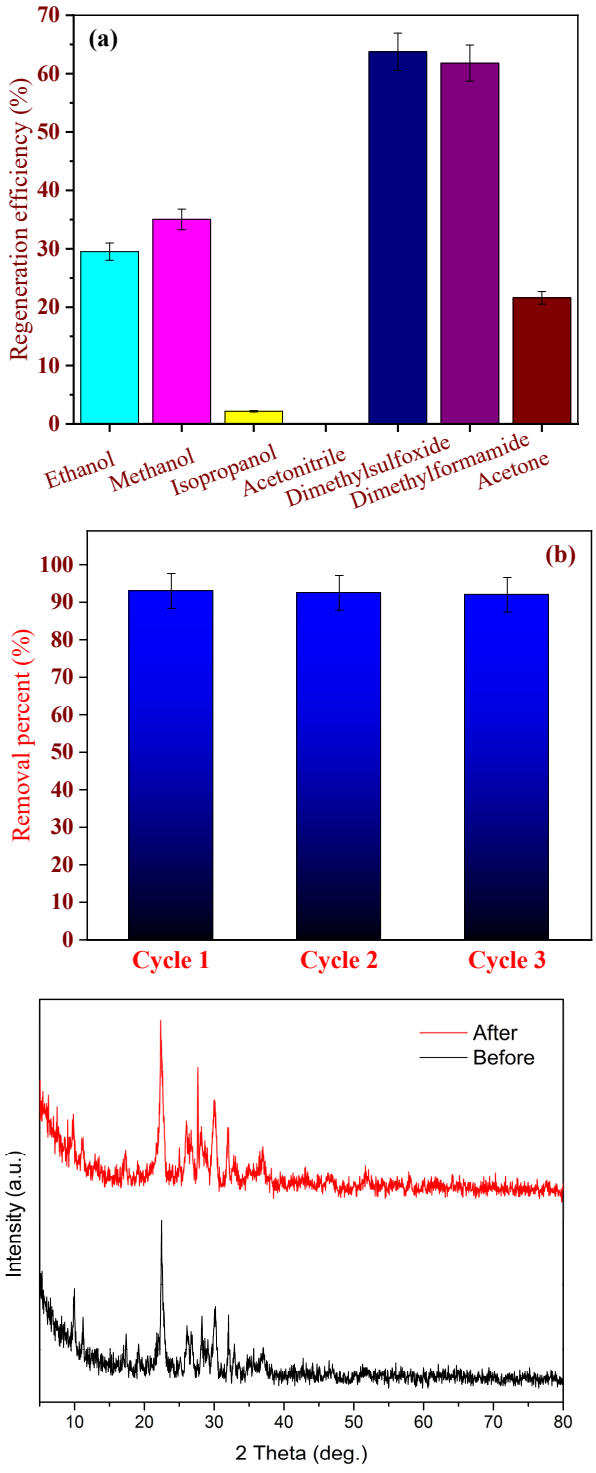

(**c**)

Figure 9. (**a**) Desorption of safinamide using different eluents, (**b**) reuse of Co/Ni/Cu-NH_2BDC MOF/zeolite nanocomposite, and (**c**) XRD diffractograms of zeolite/MOF adsorbent before and after recycling.

3.4. Adsorbent Stability and Selectivity

Adsorbent stability was assessed by soaking zeolite/MOF adsorbent in water for 24 h and collecting its XRD diffraction pattern. Figure 9c shows that no significant changes were observed for both samples, indicating the reasonable stability of this adsorbent in water effluents.

Adsorption selectivity for the safinamide drug was studied by adding 25 mg/L of different interfering species (Cl^-, NO_3^-, SO_4^{2-}, humic acid, and cefixime drug) under adsorption optimum conditions. Each of them was added separately to form a binary solution. The removal percentage for each initial concentration of the added interfering species is shown in Figure 10a. The removal percentage for interfering ions of concentrations of 100 ppm is summarized in Figure 10b. As shown in Figure 10b, the removal efficiency of safinamide was lower in nearly all binary solutions than in solutions without interfering species [80,81]. Moreover, organic compounds reduced the removal of safinamide more than inorganic compounds, where the addition of cefixime reduced the removal percentage to 34%. These results can be attributed to competition between organic compounds for the adsorption groups, and the large size of the organic structure may fill the adsorbent pores.

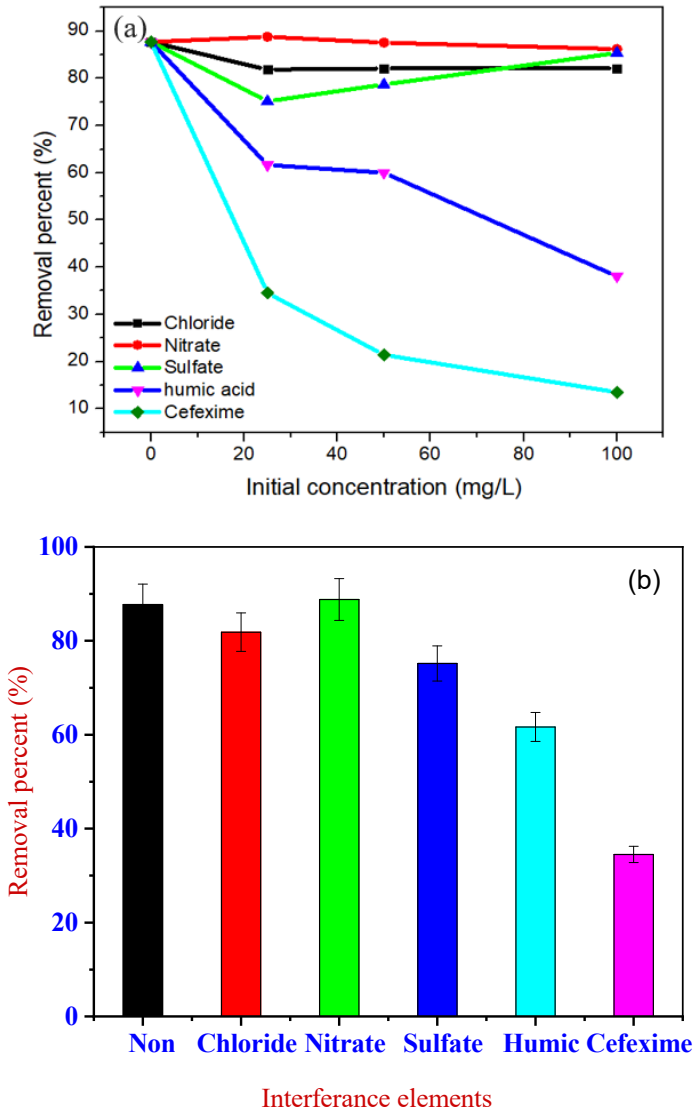

Figure 10. Removal percentage of zeolite/MOF for safinamide in the presence of different competing adsorbates (**a**) with different initial concentrations and (**b**) at 100 mg/L initial concentration.

3.5. Thermodynamic Investigation

The thermodynamic parameters for the interaction between safinamide were analyzed at different temperatures, as shown in Table 11 and Figure 11. The results indicate that the reaction is energetically favorable and spontaneous under standard conditions, with negative ΔG° values across all temperatures. The negative ΔH° suggests heat release, characteristic of an exothermic process, while the negative ΔS° indicates a decrease in disorder during the reaction. The decrease in ΔG° with increasing temperature implies reduced spontaneity at higher temperatures. Further analysis using the van't Hoff equation can provide insights into the temperature dependence and equilibrium constant (K) of the reaction [82]. Overall, the thermodynamic data reveal that the safinamide reaction is exothermic, spontaneous at room temperature, and less spontaneous at elevated temperatures.

Table 11. Thermodynamic parameters for the Cd^{2+} adsorption process.

Drug	T (K)	%R	ΔG° (KJ/mol)	ΔH° (KJ/mol)	ΔS° (J/mol K)
Safinamide	298	99	−13.1021	−118.973	−365.7329
	308	80	−5.32485		
	318	56	−2.47018		
	328	54	−2.32746		

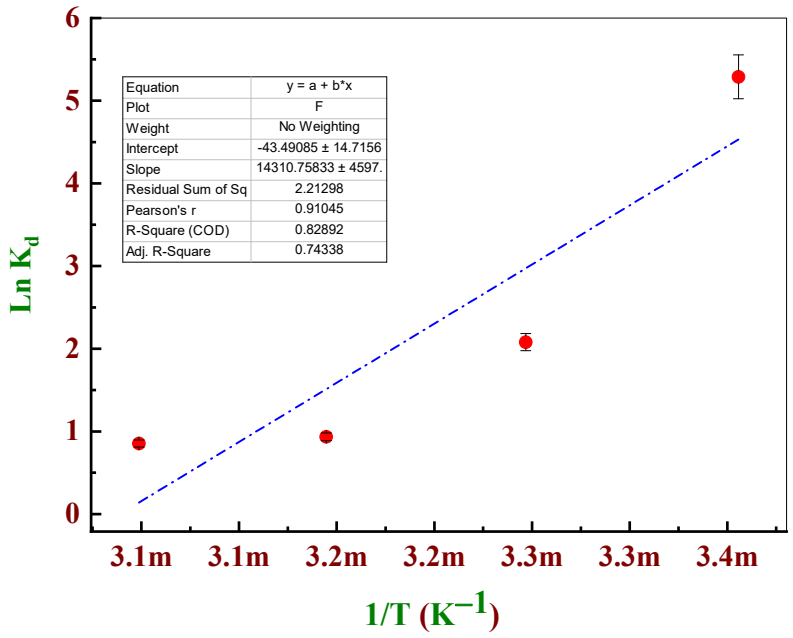

Figure 11. The study of variations in K_d with temperature enables us to estimate the thermodynamic parameters.

3.6. Real Water Sample Analysis

The removal percentage of safinamide using collected real water sources (tap water, Nile River water, and groundwater samples) by spiking 20 ppm, pH 5, and 0.10 g zeolite/MOF nanocomposite was 48.80%, 64.30%, and 44.44% for tab water, Nile River water, and groundwater, respectively.

3.7. Adsorbent Cost Analysis

Table 1 compares the maximum adsorption capacity of the prepared zeolite/MOF with similar zeolite- and MOF-based adsorbents in the literature. The current zeolite/MOF is among the highest for Cd^{2+} removal. Higher adsorption capacities are predominantly observed in adsorbents composed of MOFs as compared to zeolites. As MOF adsorbents

typically cost around USD 7/g, this may result in a probable rise in price. In contrast, zeolites generally cost approximately USD 1.5–3.5/kg, i.e., more than 1000-fold less than MOF adsorbents [83]. Other adsorbents reported in Table 1 and in recent reviews [27,30,35] showed smaller maximum adsorption capacities than the prepared zeolite/MOF.

3.8. Adsorption Mechanism

A simple mechanism for safinamide adsorption on zeolite is illustrated in Figure 12a. The molecules of this drug diffuse from the bulk of the solution to the pores of the zeolite. Due to the large size of this molecule, its diffusion is slow. When this drug is adsorbed on the active sites within the pores, the adsorption step is much faster than diffusion, leading to an internal diffusion-limited process, as discussed in the kinetics section. The drug can be adsorbed on specific active sites on the zeolite structure, which probably provides electrostatic interaction between partially negative atoms in the drug structure and partially positive sites within the zeolite framework. This leads to adsorption of a heterogeneous nature when equilibrium is reached, as discussed in the adsorption isotherm section. When MOF is added to the zeolite, the pores can get narrower, and the diffusion-limited step still controls the overall adsorption of this drug (Figure 12b). However, the MOF phase offers more active sites for this drug, probably due to hydrogen bonding and electrostatic interactions. This leads to monolayer homogenous adsorption at equilibrium, as discussed in the adsorption isotherm section.

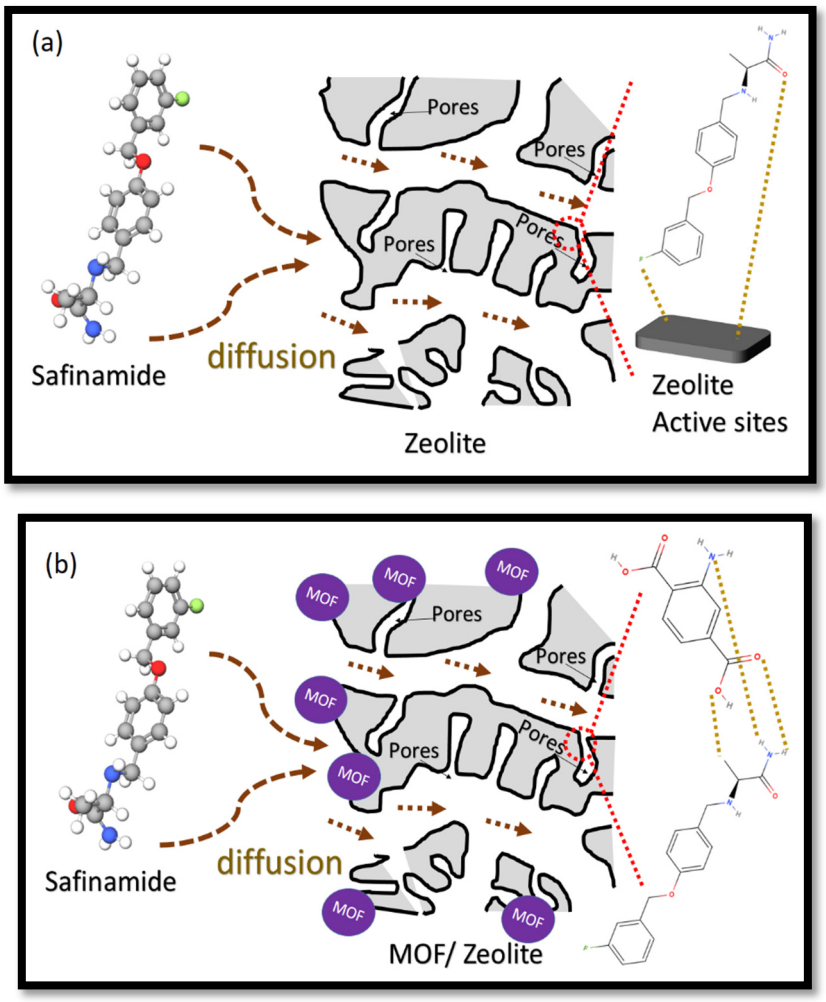

Figure 12. *Cont.*

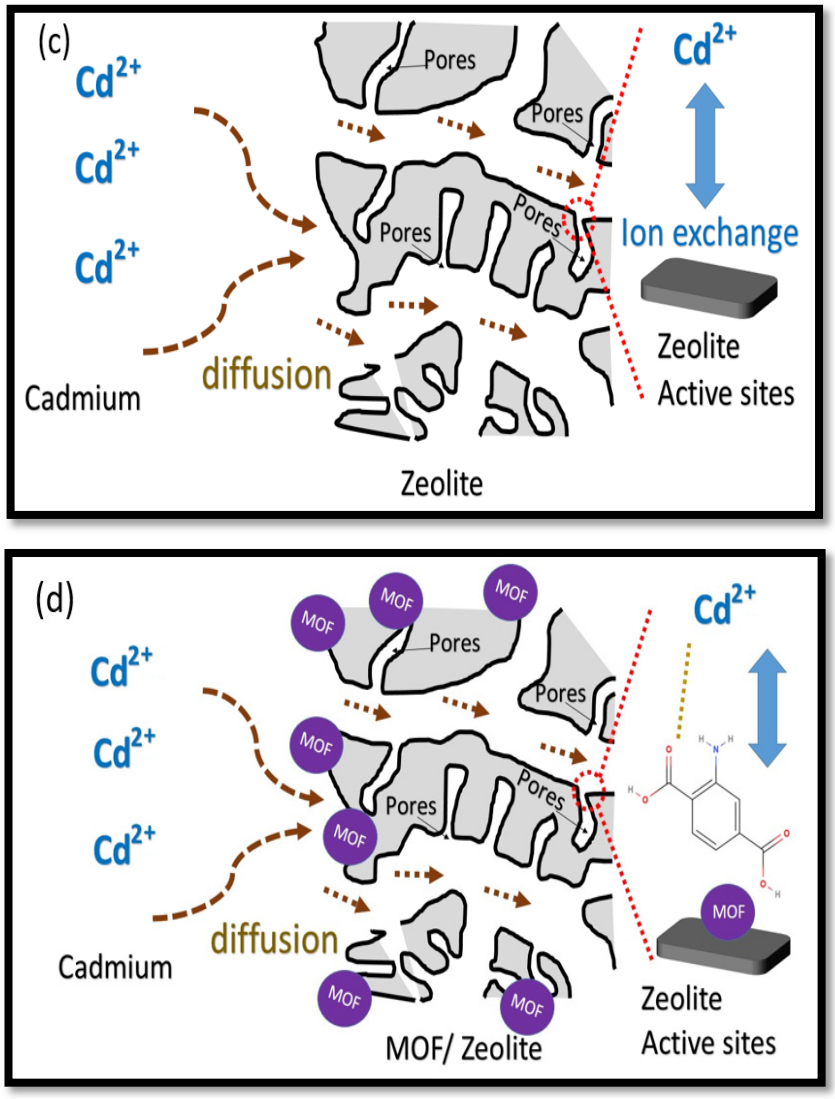

Figure 12. Possible adsorption mechanism of safinamide onto (**a**) zeolite and (**b**) zeolite/MOF and Possible adsorption mechanism of Cd onto (**c**) zeolite and (**d**) zeolite/MOF.

In the case of Cd^{2+} ions, the diffusion of such small ions is much faster, and the process is not limited to internal diffusion (Figure 12c). However, diffusion from the bulk of the solution to within the pores of zeolite can be the rate-limiting step, as reflected by the pseudo second-order kinetic model. This can be attributed to the complex nature of the pore network of zeolites, which leads to an external diffusion limitation adsorption process. When Cd^{2+} ions reach the zeolite surface, ion exchange can occur at specific sites in the zeolite framework, leading to heterogeneous adsorption in nature. When MOF is added to the zeolite phase (Figure 12d), the MOF particles can narrow the pores and lead to an internal diffusion limitation. When the MOF phase is present, part of the active sites for Cd^{2+} adsorption may be lost due to the presence of the MOF phase itself adsorbed on the surface of zeolite. This can have a negative effect on the adsorption capacity of the zeolite support. However, the MOF phase can provide interaction sites with Cd^{2+} ions, thus increasing the adsorption capacity of the overall nanocomposite. In this work, the maximum adsorption capacity for the zeolite and the zeolite/MOF were calculated to be 550.69 mg/g. This can indicate that any decrease in adsorption sites due to the presence of MOF was compensated for by its interaction with Cd^{2+}. This interaction is homogenous with monolayer adsorption, as reflected by the Langmuir isotherm model. Also, the skeleton collapsed, the material surface was no longer tightly bound, and a

significant number of amorphous particles, the majority of which may be adsorbed Cd^{2+} metal ions, attached themselves to the material surface following the adsorption reaction.

3.9. Cytotoxicity of the Investigated Adsorbent

Figure 13 shows the cytotoxic activity of the tested compounds, zeolite and zeolite/MOF, at varying concentrations as determined by MTT assays. Cytotoxicity was examined after 24 h and 48 h using a 200 µg/mL concentration. The maximum percentages of cell viability compared to untreated controls at 24 h were 83% and 81% for zeolite and zeolite/MOF, respectively. After 48 h of treatment, the cell viability compared to untreated controls was 81% and 79% for zeolite and zeolite/MOF, respectively. These cytotoxicity assays were performed in triplicate ((n = 3) ± SD). The results demonstrate that the cytotoxic activity of zeolite and zeolite/MOF at 48 h was enhanced compared to 24 h. As evidenced by the results, the cytotoxicity activity of zeolite is very close to that of zeolite/MOF and slightly lower than it.

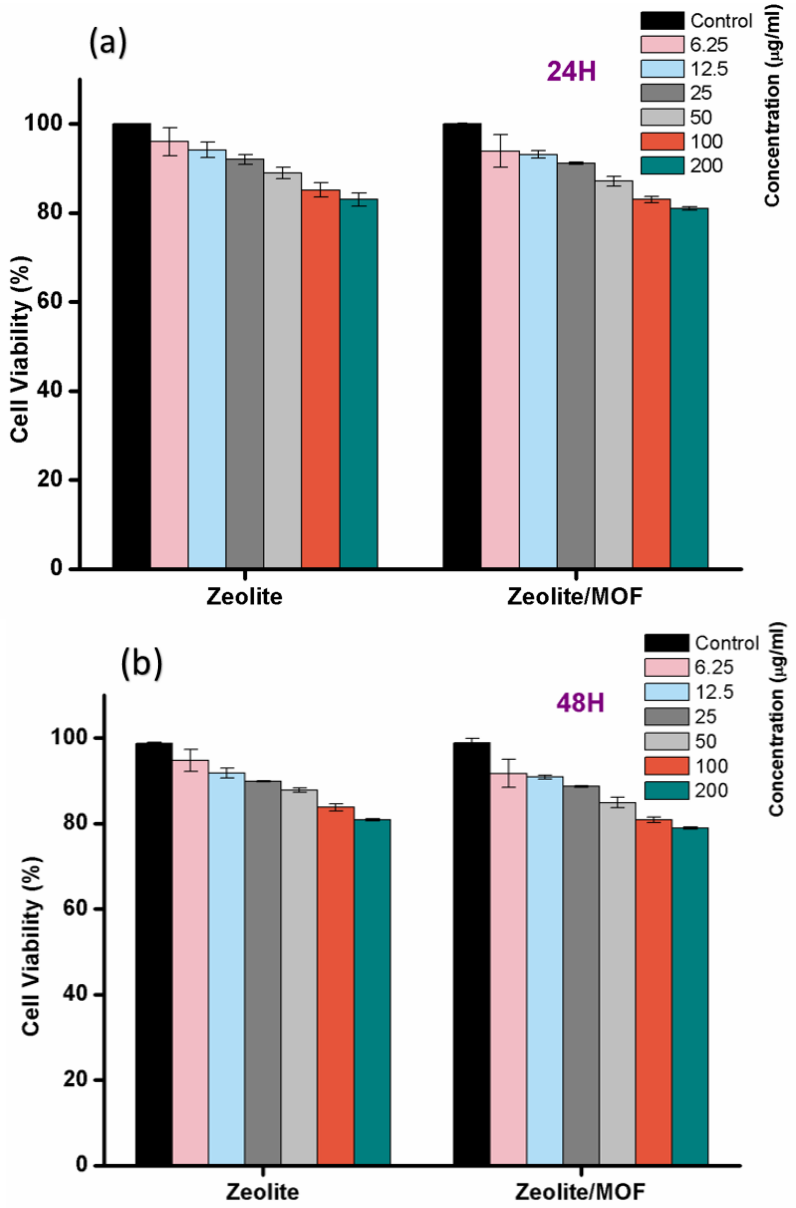

Figure 13. Cell viability (%) of zeolite and zeolite/MOF at different concentrations after (**a**) 24 h and (**b**) 48 h (n = 3) ± SD.

4. Conclusions

In this work, zeolite and its novel composite with a 2-amino terephthalic acid-based multi-metallic metal-organic framework were synthesized, involving an improvement in surface area where its value was 24.63 and 41.86 m^2/g for zeolite and zeolite/MOF, respectively. Their adsorption efficiency was best at pH 5 (48.8%) for safinamide, while for cadmium, pH 7 and 9 (48.9%) were the best for zeolite and zeolite/MOF, respectively. The maximum adsorption capacity of the zeolite/MOF composite reached 500.69 mg/g for safinamide and 550.69 mg/g for cadmium. The values of the thermodynamic parameters, i.e., Δ G°, ΔH°, and Δ S°, were established by thermodynamic studies of the removal of cadmium metal ions by zeolite/MOF. These values are very promising compared to other materials reported in the open literature. Therefore, it can be concluded that further modifications and investigations can pave the road towards an efficient adsorbent for numerous organic and inorganic applications.

Supplementary Materials: The following supporting information can be downloaded at: https://www.mdpi.com/article/10.3390/colloids8050050/s1, Figure S1: Calibration curve for Safinamide detection using UV-VIS spectrophotometer; Table S1: Isotherm models investigated in this study; Table S2: Adsorption kinetics equations investigated for non-linear regression of kinetic data.

Author Contributions: Conceptualization, R.M., A.A.F. and H.M.M.; methodology, R.M., R.A. and Z.E.E.; software, R.A., H.A.Y. and Z.E.E.; validation, R.A., H.A.Y. and Z.E.E.; formal analysis, R.M., A.A.A., H.A.R. and S.I.O.; investigation, R.M., R.A. and Z.E.E.; resources, R.M., A.A.F. and H.M.M.; data curation, R.A. and Z.E.E. and H.A.Y.; writing—original draft preparation, R.A. and Z.E.E. and H.A.Y.; writing—review and editing, R.M., A.A.F. and H.M.M.; visualization, R.M., R.A. and Z.E.E.; supervision, R.M., A.A.F. and H.M.M.; project administration, R.M., A.A.A., H.A.R. and S.I.O.; funding acquisition, A.A.A., H.A.R. and S.I.O. All authors have read and agreed to the published version of the manuscript.

Funding: This research was funded by Princess Nourah bint Abdulrahman University Researchers Supporting Project number (PNURSP2024R5), Princess Nourah bint Abdulrahman University, Riyadh, Saudi Arabia.

Data Availability Statement: The datasets used and/or analyzed during the current study are available from the corresponding author upon reasonable request.

Acknowledgments: This study/publication was made possible by the generous support of the American people through the United States Agency for International Development (USAID). The contents are the responsibility of [Rania Shaban Taha Abdelazeem] and do not necessarily reflect the views of USAID or the United States Government. In addition, this study/publication (Project ID: TAILORED ENZYMATIC AND NANO-BASED TREATMENT OF WASTEWATER TO DETOXIFY HEAVY METALS AND DEGRADE ANTIBIOTICS) was made possible by the generous support of the American people through the United States Agency for International Development (USAID). The contents are the responsibility of [Hamdaa Mahmoud] and do not necessarily reflect the views of USAID or the United States Government.

Conflicts of Interest: The authors declare no conflicts of interest.

References

1. Anfar, Z.; Zbair, M.; Ait Ahsiane, H.; Jada, A.; El Alem, N. Microwave assisted green synthesis of Fe_2O_3/biochar for ultrasonic removal of nonsteroidal anti-inflammatory pharmaceuticals. *RSC Adv.* **2020**, *10*, 11371–11380. [CrossRef] [PubMed]
2. Solanki, A.; Boyer, T.H. Pharmaceutical removal in synthetic human urine using biochar. *Environ. Sci. Water Res. Technol.* **2017**, *3*, 553–565. [CrossRef]
3. Insight into Adsorption of Combined Antibiotic-Heavy Metal Contaminants on Graphene Oxide in Water—ScienceDirect. Available online: https://www.sciencedirect.com/science/article/abs/pii/S1383586619340122 (accessed on 26 August 2024).
4. Su, Z.; Qin, F.; Zhang, H.; Huang, Z.; Guan, K.; Zheng, M.; Dai, Z.; Song, W.; Li, X. Evaluation of Developmental Toxicity of Safinamide in Zebrafish Larvae (*Danio rerio*). *Ecotoxicol. Environ. Saf.* **2023**, *262*, 115284. [CrossRef]
5. Gao, L.; Liu, Q.; Zhang, X.-R. Enhancing the Solubility and Dissolution Performance of Safinamide Using Salts. *Crystals* **2020**, *10*, 989. [CrossRef]

6. Calisto, V.; Ferreira, C.I.A.; Oliveira, J.A.B.P.; Otero, M.; Esteves, V.I. Adsorptive removal of pharmaceuticals from water by commercial and waste-based carbons. *J. Environ. Manag.* **2015**, *152*, 83–90. [CrossRef]
7. Ouyang, J.; Zhou, L.; Liu, Z.; Heng, J.Y.Y.; Chen, W. Biomass-derived activated carbons for the removal of pharmaceutical micropollutants from wastewater: A review. *Sep. Purif. Technol.* **2020**, *253*, 117536. [CrossRef]
8. Abdulkareem, A.S.; Hamzat, W.A.; Tijani, J.O.; Egbosiuba, T.C.; Mustapha, S.; Abubakre, O.K.; Okafor, B.O.; Babayemi, A.K. Isotherm, Kinetics, Thermodynamics and Mechanism of Metal Ions Adsorption from Electroplating Wastewater Using Treated and Functionalized Carbon Nanotubes. *J. Environ. Chem. Eng.* **2023**, *11*, 109180. [CrossRef]
9. Topare, N.S.; Wadgaonkar, V.S. A review on application of low-cost adsorbents for heavy metals removal from wastewater. *Mater. Today Proc.* **2023**, *77*, 8–18. [CrossRef]
10. Afroze, S.; Sen, T.K. A review on heavy metal ions and dye adsorption from water by agricultural solid waste adsorbents. *Water Air Soil Pollut.* **2018**, *229*, 225. [CrossRef]
11. Rani, L.; Kaushal, J.; Srivastav, A.L.; Mahajan, P. A critical review on recent developments in MOF adsorbents for the elimination of toxic heavy metals from aqueous solutions. *Environ. Sci. Pollut. Res.* **2020**, *27*, 44771–44796. [CrossRef]
12. Wang, S.; Hu, Y.; Wang, J. Biodegradation of typical pharmaceutical compounds by a novel strain *Acinetobacter* sp. *J. Environ. Manag.* **2018**, *217*, 240–246. [CrossRef] [PubMed]
13. Gomes, J.; Costa, R.; Quinta-Ferreira, R.M.; Martins, R.C. Application of ozonation for pharmaceuticals and personal care products removal from water. *Sci. Total Environ.* **2017**, *586*, 265–283. [CrossRef]
14. Gholami, P.; Khataee, A.; Soltani, R.D.C.; Dinpazhoh, L.; Bhatnagar, A. Photocatalytic degradation of gemifloxacin antibiotic using Zn-Co-LDH@biochar nanocomposite. *J. Hazard. Mater.* **2020**, *382*, 121070. [CrossRef] [PubMed]
15. Kamrani, M.; Akbari, A.; Yunessnia Lehi, A. Chitosan-modified acrylic nanofiltration membrane for efficient removal of pharmaceutical compounds. *J. Environ. Chem. Eng.* **2018**, *6*, 583–587. [CrossRef]
16. Barkade, S.; Sable, S.; Ashtekar, V.; Pandit, V. Removal of lead and copper from wastewater using Bael fruit shell as an adsorbent. *Mater. Today Proc.* **2022**, *53*, 65–70. [CrossRef]
17. Selective Adsorption Mechanisms of Antilipidemic and Non-Steroidal Anti-Inflammatory Drug Residues on Functionalized Silica-Based Porous Materials in a Mixed Solute—ScienceDirect. Available online: https://www.sciencedirect.com/science/article/abs/pii/S0045653515004622 (accessed on 26 August 2024).
18. Bhattacharya, A.K.; Mandal, S.N.; Das, S.K. Adsorption of Zn(II) from aqueous solution by using different adsorbents. *Chem. Eng. J.* **2006**, *123*, 43–51. [CrossRef]
19. Zheng, M.; Chen, J.; Zhang, L.; Cheng, Y.; Lu, C.; Liu, Y.; Singh, A.; Trivedi, M.; Kumar, A.; Liu, J. Metal Organic Frameworks as Efficient Adsorbents for Drugs from Wastewater. *Mater. Today Commun.* **2022**, *31*, 103514. [CrossRef]
20. Mansouri, H.; Carmona, R.J.; Gomis-Berenguer, A.; Souissi-Najar, S.; Ouederni, A.; Ania, C.O. Competitive Adsorption of Ibuprofen and Amoxicillin Mixtures from Aqueous Solution on Activated Carbons. *J. Colloid Interface Sci.* **2015**, *449*, 252–260. [CrossRef]
21. Huang, D.; Wu, J.; Wang, L.; Liu, X.; Meng, J.; Tang, X.; Tang, C.; Xu, J. Novel Insight into Adsorption and Co-Adsorption of Heavy Metal Ions and an Organic Pollutant by Magnetic Graphene Nanomaterials in Water. *Chem. Eng. J.* **2019**, *358*, 1399–1409. [CrossRef]
22. Zhou, Y.; He, Y.; Xiang, Y.; Meng, S.; Liu, X.; Yu, J.; Yang, J.; Zhang, J.; Qin, P.; Luo, L. Single and Simultaneous Adsorption of Pefloxacin and Cu(II) Ions from Aqueous Solutions by Oxidized Multiwalled Carbon Nanotube. *Sci. Total Environ.* **2019**, *646*, 29–36. [CrossRef]
23. Wang, Y.; Wang, X.; Li, J.; Li, Y.; Xia, S.; Zhao, J.; Minale, T.M.; Gu, Z. Coadsorption of Tetracycline and Copper(II) onto Struvite Loaded Zeolite—An Environmentally Friendly Product Recovered from Swine Biogas Slurry. *Chem. Eng. J.* **2019**, *371*, 366–377. [CrossRef]
24. Shen, Y.; Sun, P.; Ye, L.; Xu, D. Progress of anaerobic membrane bioreactor in municipal wastewater treatment. *Sci. Adv. Mater.* **2023**, *15*, 1277–1298. [CrossRef]
25. Akhtar, F.; Andersson, L.; Ogunwumi, S.; Hedin, N.; Bergström, L. Structuring adsorbents and catalysts by processing of porous powders. *J. Eur. Ceram. Soc.* **2014**, *34*, 1643–1666. [CrossRef]
26. Velarde, L.; Nabavi, M.S.; Escalera, E.; Antti, M.-L.; Akhtar, F. Adsorption of heavy metals on natural zeolites: A review. *Chemosphere* **2023**, *328*, 138508. [CrossRef] [PubMed]
27. Tran, L.; Wu, P.; Zhu, Y.; Yang, L.; Zhu, N. Highly enhanced adsorption for the removal of Hg(II) from aqueous solution by Mercaptoethylamine/Mercaptopropyltrimethoxysilane functionalized vermiculites. *J. Colloid Interface Sci.* **2015**, *445*, 348–356. [CrossRef]
28. Ul Mehdi, S.; Aravamudan, K. Adsorption of cadmium ions on silica coated metal organic framework. *Mater. Today Proc.* **2022**, *61*, 487–497. [CrossRef]
29. Nabipour, H.; Rohani, S.; Batool, S.; Yusuff, A.S. An overview of the use of water-stable metal-organic frameworks in the removal of cadmium ion. *J. Environ. Chem. Eng.* **2023**, *11*, 109131. [CrossRef]
30. Abdel-Magied, A.F.; Abdelhamid, H.N.; Ashour, R.M.; Fu, L.; Dowaidar, M.; Xia, W.; Forsberg, K. Magnetic Metal-Organic Frameworks for Efficient Removal of Cadmium(II), and Lead(II) from Aqueous Solution. *J. Environ. Chem. Eng.* **2022**, *10*, 107467. [CrossRef]

31. Mahmoud, M.E.; Amira, M.F.; Seleim, S.M.; Mohamed, A.K. Amino-decorated magnetic metal-organic framework as a potential novel platform for selective removal of chromium (Vl), cadmium (II) and lead (II). *J. Hazard. Mater.* **2020**, *381*, 120979. [CrossRef]
32. Kalantar, Z.; Ghanavati Nasab, S. Modeling and optimizing Cd(II) ions adsorption onto Corn Silk/Zeolite-Y composite from industrial effluents applying response surface methodology: Isotherm, kinetic, and reusability studies. *J. Iran. Chem. Soc.* **2022**, *19*, 4209–4221. [CrossRef]
33. Synthesis of Zeolitic Imidazolate Framework-8 (ZIF-8) Using Different Solvents for Lead and Cadmium Adsorption | Applied Nanoscience. Available online: https://link.springer.com/article/10.1007/s13204-022-02680-7 (accessed on 26 August 2024).
34. Mansoorianfar, M.; Nabipour, H.; Pahlevani, F.; Zhao, Y.; Hussain, Z.; Hojjati-Najafabadi, A.; Hoang, H.Y.; Pei, R. Recent Progress on Adsorption of Cadmium Ions from Water Systems Using Metal-Organic Frameworks (MOFs) as an Efficient Class of Porous Materials. *Environ. Res.* **2022**, *214*, 114113. [CrossRef] [PubMed]
35. Yusuff, A.S.; Popoola, L.T.; Babatunde, E.O. Adsorption of cadmium ion from aqueous solutions by copper-based metal organic framework: Equilibrium modeling and kinetic studies. *Appl. Water Sci.* **2019**, *9*, 106. [CrossRef]
36. Peng, Z.; Lin, X.; Zhang, Y.; Hu, Z.; Yang, X.; Chen, C.; Chen, H.; Li, Y.; Wang, J. Removal of Cadmium from Wastewater by Magnetic Zeolite Synthesized from Natural, Low-Grade Molybdenum. *Sci. Total Environ.* **2021**, *772*, 145355. [CrossRef]
37. Abdelmoaty, A.S.; El-Wakeel, S.T.; Fathy, N.; Hanna, A.A. High Performance of UiO-66 Metal–Organic Framework Modified with Melamine for Uptaking of Lead and Cadmium from Aqueous Solutions. *J. Inorg. Organomet. Polym. Mater.* **2022**, *32*, 2557–2567. [CrossRef]
38. Roushani, M.; Saedi, Z.; Baghelani, Y.M. Removal of cadmium ions from aqueous solutions using TMU-16-NH 2 metal organic framework. *Environ. Nanotechnol. Monit. Manag.* **2017**, *7*, 89–96. [CrossRef]
39. Liang, Z.; Gao, Q.; Wu, Z.; Gao, H. Removal and kinetics of cadmium and copper ion adsorption in aqueous solution by zeolite NaX synthesized from coal gangue. *Environ. Sci. Pollut. Res.* **2022**, *29*, 84651–84660. [CrossRef]
40. Shawabkeh, R.; Al-Harahsheh, A.; Hami, M.; Khlaifat, A. Conversion of oil shale ash into zeolite for cadmium and lead removal from wastewater. *Fuel* **2004**, *83*, 981–985. [CrossRef]
41. Wang, Y.; Ye, G.; Chen, H.; Hu, X.; Niu, Z.; Ma, S. Functionalized Metal–Organic Framework as a New Platform for Efficient and Selective Removal of Cadmium(II) from Aqueous Solution. *J. Mater. Chem. A* **2015**, *3*, 15292–15298. [CrossRef]
42. Jorfi, S.; Shooshtarian, M.R.; Pourfadakari, S. Decontamination of cadmium from aqueous solutions using zeolite decorated by Fe_3O_4 nanoparticles: Adsorption modeling and thermodynamic studies. *Int. J. Environ. Sci. Technol.* **2020**, *17*, 273–286. [CrossRef]
43. Gutiérrez-Segura, E.; Solache-Ríos, M.; Colín-Cruz, A.; Fall, C. Adsorption of cadmium by Na and Fe modified zeolitic tuffs and carbonaceous material from pyrolyzed sewage sludge. *J. Environ. Manag.* **2012**, *97*, 6–13. [CrossRef]
44. Merrikhpour, H.; Jalali, M. Comparative and competitive adsorption of cadmium, copper, nickel, and lead ions by Iranian natural zeolite. *Clean Technol. Environ. Policy* **2013**, *15*, 303–316. [CrossRef]
45. El-Shafie, A.S.; Rahman, E.; GadelHak, Y.; Mahmoud, R.; El-Azazy, M. Techno-economic assessment of waste mandarin biochar as a green adsorbent for binary dye wastewater effluents of methylene blue and basic fuchsin: Lab- and large-scale investigations. *Spectrochim. Acta Part A Mol. Biomol. Spectrosc.* **2024**, *306*, 123621. [CrossRef] [PubMed]
46. Treatment of CrVI-Containing $Mg(OH)_2$ Nanowaste—Liu—2008—Angewandte Chemie—Wiley Online Library. Available online: https://onlinelibrary.wiley.com/doi/full/10.1002/ange.200800172 (accessed on 26 August 2024).
47. GadelHak, Y.; Salama, E.; Abd-El Tawab, S.; Mouhmed, E.A.; Alkhalifah, D.H.M.; Hozzein, W.N.; Mohaseb, M.; Mahmoud, R.K.; Amin, R.M. Waste Valorization of a Recycled ZnCoFe Mixed Metal Oxide/Ceftriaxone Waste Layered Nanoadsorbent for Further Dye Removal. *ACS Omega* **2022**, *7*, 44103–44115. [CrossRef] [PubMed]
48. Microorganisms | Free Full-Text | Controlling Multi-Drug-Resistant Traits of Salmonella Obtained from Retail Poultry Shops Using Metal–Organic Framework (MOF) as a Novel Technique. Available online: https://www.mdpi.com/2076-2607/11/10/2506 (accessed on 26 August 2024).
49. Nagalakshmi, G.; Nandeesh, I.M.; Yallur, B.C.; Adimule, V.; Batakurki, S. Synthesis and Optical Properties of Copper Terephthalate Metal Organic Frame Works. *Eng. Chem.* **2023**, *2*, 3–11. [CrossRef]
50. Gokila, N.; Muthumalai, K.; Haldorai, Y.; Kumar, R.T.R. Electrochemical Non-enzymatic sensor based on Co-H_2ABDC Metal Organic Framework for detection of glyphosate. *Chem. Phys. Lett.* **2022**, *795*, 139481. [CrossRef]
51. Holzwarth, U.; Gibson, N. The Scherrer equation versus the "Debye-Scherrer equation". *Nat. Nanotechnol.* **2011**, *6*, 534. [CrossRef] [PubMed]
52. Cheng, T.C.; Bandyopadhyay, B.; Mosley, J.D.; Duncan, M.A. IR spectroscopy of protonation in benzene-water nanoclusters: Hydronium, zundel, and eigen at a hydrophobic interface. *J. Am. Chem. Soc.* **2012**, *134*, 13046–13055. [CrossRef]
53. Sarabadan, M.; Bashiri, H.; Mousavi, S.M. Adsorption of crystal violet dye by a zeolite-montmorillonite nano-adsorbent: Modelling, kinetic and equilibrium studies. *Clay Miner.* **2019**, *54*, 357–368. [CrossRef]
54. Water | Free Full-Text | Chromium Removal from Aqueous Solution Using Natural Clinoptilolite. Available online: https://www.mdpi.com/2073-4441/15/9/1667 (accessed on 26 August 2024).
55. Naikoo, R.A.; Bhat, S.U.; Mir, M.A.; Tomar, R.; Khanday, W.A.; Dipak, P.; Tiwari, D.C. Polypyrrole and Its Composites with Various Cation Exchanged Forms of Zeolite X and Their Role in Sensitive Detection of Carbon Monoxide. *RSC Adv.* **2016**, *6*, 99202–99210. [CrossRef]
56. Dehghan, A.; Zarei, A.; Jaafari, J.; Shams, M.; Khaneghah, A.M. Tetracycline removal from aqueous solutions using zeolitic imidazolate frameworks with different morphologies: A mathematical modeling. *Chemoshphere* **2019**, *217*, 250–260. [CrossRef]

57. Karge, H.G.; Weitkamp, J. (Eds.) *Characterization I*; Molecular Sieves; Springer: Berlin/Heidelberg, Germany, 2004; pp. 1–540.
58. Rezaei Kahkha, M.R.; Oveisi, A.R.; Kaykhaii, M.; Rezaei Kahkha, B. Determination of carbamazepine in urine and water samples using amino-functionalized metal–organic framework as sorbent. *Chem. Cent. J.* **2018**, *12*, 77. [CrossRef] [PubMed]
59. Matin, M.A.; Bhattacharjee, S.; Shaikh, M.A.A.; Debnath, T.; Aziz, M.A. A Density Functional Theory (DFT) Investigation on the Structure and Spectroscopic Behavior of 2-Aminoterephthalic Acid and Its Sodium Salts. *Green Sustain. Chem.* **2020**, *10*, 39. [CrossRef]
60. Mehdinia, A.; Mollazadeh-Moghaddam, A.; Jabbari, A. Fabrication of Silver–2–Aminoterephthalic Acid Coordination Polymer-Coated Fe_3O_4 for Effective Removal of Lead from Aqueous Media. *Int. J. Environ. Res.* **2021**, *15*, 631–644. [CrossRef]
61. Isaeva, V.I.; Timofeeva, M.N.; Lukoyanov, I.A.; Gerasimov, E.Y.; Panchenko, V.N.; Chernyshev, V.V.; Glukhov, L.M.; Kustov, L.M. Novel MOF Catalysts Based on Calix[4]Arene for the Synthesis of Propylene Carbonate from Propylene Oxide and CO_2. *J. CO_2 Util.* **2022**, *66*, 102262. [CrossRef]
62. Natarajan, T.S.; Bajaj, H.C.; Tayade, R.J. Preferential adsorption behavior of methylene blue dye onto surface hydroxyl group enriched TiO_2 nanotube and its photocatalytic regeneration. *J. Colloid Interface Sci.* **2014**, *433*, 104–114. [CrossRef] [PubMed]
63. Thommes, M.; Kaneko, K.; Neimark, A.V.; Olivier, J.P.; Rodriguez-Reinoso, F.; Rouquerol, J.; Sing, K.S.W. Physisorption of Gases, with Special Reference to the Evaluation of Surface Area and Pore Size Distribution (IUPAC Technical Report). *Pure Appl. Chem.* **2015**, *87*, 1051–1069. [CrossRef]
64. Desaphy, J.-F.; Farinato, A.; Altamura, C.; De Bellis, M.; Imbrici, P.; Tarantino, N.; Caccia, C.; Melloni, E.; Padoani, G.; Vailati, S.; et al. Safinamide's Potential in Treating Nondystrophic Myotonias: Inhibition of Skeletal Muscle Voltage-Gated Sodium Channels and Skeletal Muscle Hyperexcitability In Vitro and In Vivo. *Exp. Neurol.* **2020**, *328*, 113287. [CrossRef]
65. Chauhan, D.; Jaiswal, M.; Sankararamakrishnan, N. Removal of cadmium and hexavalent chromium from electroplating waste water using thiocarbamoyl chitosan. *Carbohydr. Polym.* **2012**, *88*, 670–675. [CrossRef]
66. Purna Chandra Rao, G.; Satyaveni, S.; Ramesh, A.; Seshaiah, K.; Murthy, K.S.N.; Choudary, N.V. Sorption of Cadmium and Zinc from Aqueous Solutions by Zeolite 4A, Zeolite 13X and Bentonite. *J. Environ. Manage.* **2006**, *81*, 265–272. [CrossRef]
67. Vedula, S.S.; Yadav, G.D. Wastewater treatment containing methylene blue dye as pollutant using adsorption by chitosan lignin membrane: Development of membrane, characterization and kinetics of adsorption. *J. Indian Chem. Soc.* **2022**, *99*, 100263. [CrossRef]
68. Ohale, P.E.; Onu, C.E.; Ohale, N.J.; Oba, S.N. Adsorptive kinetics, isotherm and thermodynamic analysis of fishpond effluent coagulation using chitin derived coagulant from waste *Brachyura* shell. *Chem. Eng. J. Adv.* **2020**, *4*, 100036. [CrossRef]
69. Ma, Y.; Jamili, A. Modeling the density profiles and adsorption of pure and mixture hydrocarbons in shales. *J. Unconv. Oil Gas Resour.* **2016**, *14*, 128–138. [CrossRef]
70. Podder, M.S.; Majumder, C.B. Studies on the removal of As(III) and As(V) through their adsorption onto granular activated carbon/$MnFe_2O_4$ composite: Isotherm studies and error analysis. *Compos. Interfaces* **2016**, *23*, 327–372. [CrossRef]
71. Syafiuddin, A.; Salmiati, S.; Jonbi, J.; Fulazzaky, M.A. Application of the kinetic and isotherm models for better understanding of the behaviors of silver nanoparticles adsorption onto different adsorbents. *J. Environ. Manag.* **2018**, *218*, 59–70. [CrossRef] [PubMed]
72. Ramadoss, R.; Subramaniam, D. Removal of divalent nickel from aqueous solution using blue-green marine algae: Adsorption modeling and applicability of various isotherm models. *Sep. Sci. Technol.* **2019**, *54*, 943–961. [CrossRef]
73. Fritz, W.; Schluender, E.-U. Simultaneous adsorption equilibria of organic solutes in dilute aqueous solutions on activated carbon. *Chem. Eng. Sci.* **1974**, *29*, 1279–1282. [CrossRef]
74. Renewable Conversion of Coal Gangue to 13-X Molecular Sieve for Cd^{2+}-Containing Wastewater Adsorption Performance | Rare Metals. Available online: https://link.springer.com/article/10.1007/s12598-023-02461-3 (accessed on 26 August 2024).
75. Lin, G.; Zeng, B.; Li, J.; Wang, Z.; Wang, S.; Hu, T.; Zhang, L. A Systematic Review of Metal Organic Frameworks Materials for Heavy Metal Removal: Synthesis, Applications and Mechanism. *Chem. Eng. J.* **2023**, *460*, 141710. [CrossRef]
76. Wang, J.; Guo, X. Adsorption kinetic models: Physical meanings, applications, and solving methods. *J. Hazard. Mater.* **2020**, *390*, 122156. [CrossRef]
77. Ebelegi, A.N.; Ayawei, N.; Wankasi, D. Interpretation of adsorption thermodynamics and kinetics. *Open J. Phys. Chem.* **2020**, *10*, 166–182. [CrossRef]
78. Hubbe, M.A.; Azizian, S.; Douven, S. Implications of apparent pseudo-second-order adsorption kinetics onto cellulosic materials: A review. *BioResources* **2019**, *14*, 7582–7626. [CrossRef]
79. Verma, B. *Phytoremediation of Heavy Metals, Soil Health Impacts and Productivity of Calendula (Calendula officinalis L.) under Irrigation with Heavy Metals Spiked Wastewater*; Water Science and Technology Icar-Indian Agricultural Research Institute: New Delhi, India, 2022.
80. Bezerra de Araujo, C.M.; Wernke, G.; Ghislandi, M.G.; Diório, A.; Vieira, M.F.; Bergamasco, R.; Alves da Motta Sobrinho, M.; Rodrigues, A.E. Continuous Removal of Pharmaceutical Drug Chloroquine and Safranin-O Dye from Water Using Agar-Graphene Oxide Hydrogel: Selective Adsorption in Batch and Fixed-Bed Experiments. *Environ. Res.* **2023**, *216*, 114425. [CrossRef] [PubMed]
81. Metal Organic Framework–Derived Recyclable Magnetic Coral Co@Co_3O_4/C for Adsorptive Removal of Antibiotics from Wastewater | Environmental Science and Pollution Research. Available online: https://link.springer.com/article/10.1007/s11356-023-25846-4 (accessed on 26 August 2024).

82. Abdel-Hady, E.E.; Mahmoud, R.; Hafez, S.H.M.; Mohamed, H.F.M. Hierarchical ternary ZnCoFe layered double hydroxide as efficient adsorbent and catalyst for methanol electrooxidation. *J. Mater. Res. Technol.* **2022**, *17*, 1922–1941. [CrossRef]
83. GadelHak, Y.; El-Azazy, M.; Shibl, M.F.; Mahmoud, R.K. Cost estimation of synthesis and utilization of nano-adsorbents on the laboratory and industrial scales: A detailed review. *Sci. Total Environ.* **2023**, *875*, 162629. [CrossRef] [PubMed]